To the Graduate Council:

I am submitting herewith a thesis written by Daniel Steven Daniel entitled "Advanced Diamond Machining: Modeling, Simulation and Control." I have examined the final copy of this thesis for form and content and recommend that it be accepted in partial fulfillment of the requirements for the degree of Master of Science, with a major in Electrical Engineering.

J.M. Bailey, Major Professor

We have read this thesis
and recommend its acceptance:

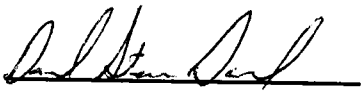
Accepted for the Council:

Associate Vice Chancellor
and Dean of the Graduate School

STATEMENT OF PERMISSION OF USE

In presenting this thesis in partial fulfillment of the requirements for a Master's degree at The University of Tennessee, Knoxville, I agree that the Library shall make it available to borrowers under the rules of the Library. Brief quotations from this thesis are allowable without special permission, provided that accurate acknowledgement of the source is made.

Permission for extensive quotation from or reproduction of this thesis may be granted by my major professor, or in his absence, by the Head of Interlibrary Services when, in the opinion of either, the proposed use of the material is for scholarly purposes. Any copying or use of the material in this thesis for financial gain shall not be allowed without my written permission.

Signature 

Date 12/2/93

ADVANCED DIAMOND MACHINING:

MODELING, SIMULATION AND CONTROL

A Thesis

Presented for the

Master of Science

Degree

The University of Tennessee, Knoxville

Daniel Steven Daniel

December 1993

ACKNOWLEDGEMENTS

First and foremost, I would like to thank my wonderful wife Anamary for her selflessness and infinite patience. I must also give great thanks to Dr. J. Milton Bailey for his continued support and influence while pursuing my graduate studies. To the University of Tennessee, I give thanks for allowing me to continue my studies in Electrical Engineering and for providing the much needed financial support.

I certainly wish to recognize the support of the Department of Energy and Martin Marietta Energy Systems for funding this thesis under contract MMES 7685PAY34. I would like to also give thanks to my colleagues at the Advanced Technology Division of Martin Marietta Energy Systems for their assistance and suggestions while preparing this thesis. Finally, I wish to thank my father John L. Daniel for providing me with not only educational opportunities, but also the proper upbringing to utilize the knowledge gained in a positive and productive manner.

ABSTRACT

The objective of this thesis was to model and to design a control for a large turning machine which utilizes a diamond tool bit. The emphasis of the thesis was on accurately modeling the dynamics of the system and to determine whether the machine, as it is described, can be controlled to produce the desired surface finish. The control design was performed using classical techniques, and simulated using state equations. The use of computer aided design tools, MATLAB and SIMNON, were used extensively to perform much of the analysis and simulation. Two simulations were be performed, one for the linear system and one including known disturbance sources as well as system non-linearity. The results of the simulations will be used to illuminated the effectiveness and the weakness of the control structure. Suggestions were made as to parametric changes that may be implemented to produce the best possible surface finish with minimal control effort.

TABLE OF CONTENTS

CHAPTER		PAGE
1	INTRODUCTION	1
2	MODELING OF THE DYNAMIC SYSTEM	5
	2-1. Introduction	5
	2-2. Linear to Rotary Motion Transformation	6
	2-3. Derivation of the System Equations	7
	2-4. Derivation of the State Equations	10
	2-5. Laplace Domain Representation of the System	14
	2-6. Block Diagram Construction	15
	2-7. Rotary to Linear Motion Transformation	19
	2-8. System Feedback	20
	2-9. System Parameters	21
	2-10. Derivation of Load Torque Expression	26
3	CONTROL OF THE DYNAMIC SYSTEM	33
	3-1. Introduction	33
	3-2. Specifications	34
	3-3. Error Analysis	35
	3-4. Closed Loop Response	38
	3-5. Controller Design	39
	3-6 Effect of Control on Root Locus	46
4	SYSTEM SIMULATION	48
	4-1. Overview	48
	4-2. Practical Implementation of Cascade Controller	48
5	SYSTEM SIMULATION: SECOND ORDER EFFECTS	54
	5-1. Derivation of Ripple Torque Equation	54
	5-2. Backlash and Saturation Equations	56
	5-3. Addition of Disturbance Torque	56
	5-4. Addition of Ripple Torque	58
	5-5. Addition of Backlash and Saturation	58
	5-6. Motor Constraints	59

6 CONCLUSION 61

LIST OF REFERENCES 63

APPENDICES

APPENDIX A 66

APPENDIX B 71

VITA 82

LIST OF FIGURES

FIGURE		PAGE
1-1	Diamond turning machine	2
1-2	Toolholder assembly	3
2-1	Model transformation	7
2-2	Free body diagrams	7
2-3	Simulation diagram	13
2-4	S-domain block diagram	16
2-5	Complete block diagram	22
2-6	Free body diagram of tool holder	27
2-7	Leadscrew thread analysis	29
2-8	Load torque graph	31
3-1	Block diagram of closed loop system	35
3-2	Step response of system with gain added	40
3-3	Ramp response of system with gain added	41
3-4	Pole-zero plot	44
3-5	Root locus plot of uncompensated system	46
3-6	Root locus plot of compensated system	47
4-1	Response due to step function input: (a) Position response, (b) Error response	49
4-2	Response due to step function input: (a) Motor Current, (b) Steady State error	49

4-3	Response due to ramp function input: (a) Position response, (b) Error response	50
4-4	Response due to ramp function input: (a) Motor current, (b) Steady State error	50
4-5	Practical implementation of controller	52
4-6	Gain plot of controller transfer function	53
4-7	Phase plot of controller transfer function	53
5-1	Ripple torque	54
5-2	Error response due to ramp function input: (a) error response, (b) expanded error response	57
5-3	Response due to ramp function input: (a) Motor current, (b) Motor power	60
A-1	Tool holder position with ramp function input	67
A-2	Tool holder position with step function input	68
A-3	Error response due to step function input (a) Error, (b) Expanded error	69
A-4	Response due to step function input (a) Motor current, (b) Motor power	70

CHAPTER 1

INTRODUCTION

Diamond Machining is a process in which a precision diamond cutting tool is used as the tool bit in a fixed part-moving tool machining operation. The operation of the machine is similar to that of a variable radius flycutting operation or an inverted metal turning operation [1] . The tool holder is mounted on a horizontal slide which is rotated at approximately 100 rpm by a large spindle shaft and counterbalanced by injecting mercury into vessels mounted on the horizontal bar. The position of the tool holder will be fed back to the controller by utilizing a laser interferometer. An isometric drawing of the machine is shown in Figure 1-1. The use of a diamond cutting tool provides for a machined finish far superior to any other type of a cutting tool such as a carbide cutting bit .

The fine machining of metal has been accomplished in the past by making rough cuts of the surface and then finishing the surface by hand lapping. This type of hand lapping is extremely labor intensive and inefficient. Thus, a machine able to provide the user with a specified surface finish without laborious hand operations would be of benefit. A mock machine for this purpose has been designed and assembled [2].

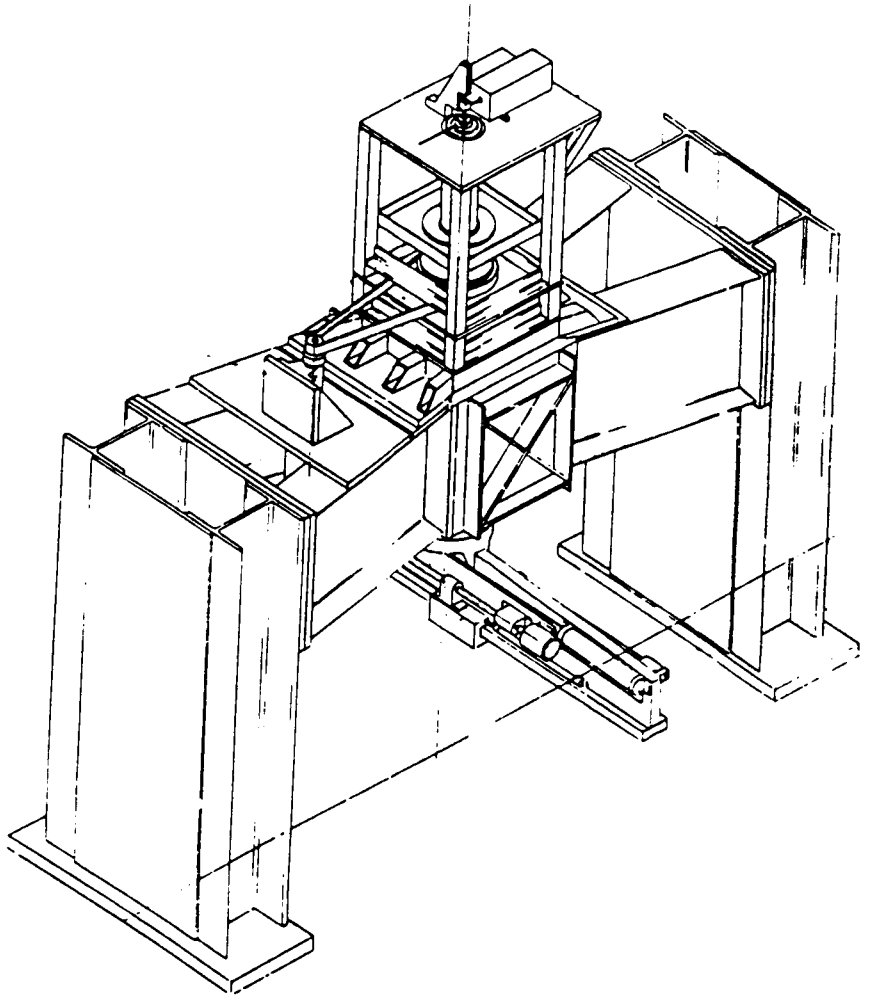


Figure 1-1, Diamond turning machine.

Mounted on the horizontal bar is the tool holder, leadscrew, servomotor, interferometer mirrors, and the balancing vessels. The servomotor receives its power via slip rings which are connected to the controller. The controller applies voltage to the armature of the permanent-magnet servomotor which rotates the motor shaft and leadscrew. The leadscrew is used to transform the rotary motion of the motor into a linear motion of the tool holder.

The analysis and design process will begin with the modeling of the servomotor, the leadscrew, and the tool holder and any interacting dynamics of the system. This assembly is shown in Figure 1-2. Once the system equations are derived, it can be seen that the system is of a nonlinear type. For the preliminary analysis and control design the system will be considered to be linear-time invariant. This assumption will facilitate the use of classical control theory to design a position controller to produce the desired surface finish on the machined part.

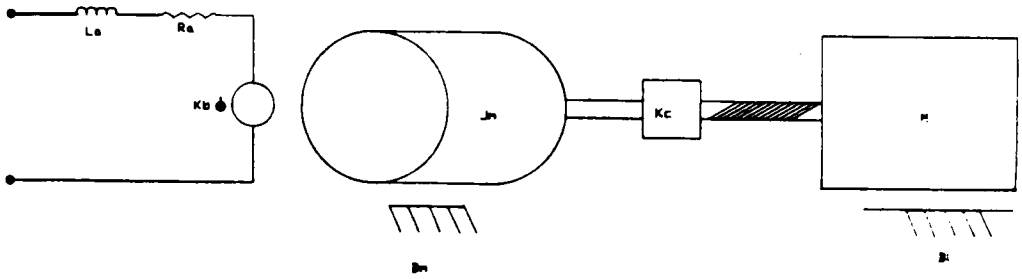


Figure 1-2, Toolholder assembly.

Once the dynamics of the machine are modeled, the equations of state will be used to develop a computer code to perform an open loop simulation using PC-SIMNON; this is to verify the machine model [3] . The equations of state and subsequently the Laplace domain equations will be utilized to develop a control algorithm. This control algorithm

will be simulated with the machine dynamics in a closed loop fashion. At this point any modifications to the closed loop response of the system will be made. Once the desired closed loop response is achieved a second simulation will be performed to account for nonlinear and secondary effects such as ripple torque, backlash and saturation. Again, modifications to the control algorithm will be made to assure the best surface finish possible.

CHAPTER 2

MODELING OF THE DYNAMIC SYSTEM

2-1 Introduction

The modeling of the machine or the process is the most important part of any control system study. Without an accurate model of the system, any compensation that may be designed for the system may not produce the desired response. The system is generally modeled by writing algebraic and differential equations which describe the physical process that is taking place, these equations may be linear or non-linear depending on the process.

To model the diamond turning machine, the well known laws of Newtonian mechanics are employed. The first step in the process is to assure that all of the energy storage elements (i.e. mass or inertia) are translated into the same reference plane. In Diamond Turning Machine; hereafter, abbreviated as DTM, the mass of the tool holder must be transformed into an inertia. The servomotor will "see" the mass of the tool holder as an inertia, this translation will place the energy storage components into the same reference plane. The next step in the modeling process is to construct free-body diagrams that describe the complete assembly. An alternate technique is to use the force-voltage or force-current analogies to create equivalent electrical circuits which are then solved by nodal or mesh analysis.

From the free-body diagrams, the differential equations that describe the dynamic system can be written. The differential equations that are written from the free body diagrams do

not account for system non-linearity; thus, algebraic expressions must be written to include the system perturbations and non-linearity. To be consistent with the prior research at Y-12, the English form of units will be throughout this thesis.

2-2. Linear to Rotary Motion Transformation

To transform the tool holder mass into an inertia reflected to the load, the tool holder is treated as a point mass on a pulley system. The equation that is employed to perform this transformation appears in many references and will not be derived [4] . This transformation is accomplished by the use of eq. (2-1),

$$J=\frac{W}{g}\left(\frac{L}{2\pi}\right)^2 \qquad (2\text{-}1)$$

where in the British system of units.

J= inertia (oz-in.-sec^2)

W= weight (oz)

L= screw lead (in.)

g= gravitational force (386.4 in./sec^2)

After this transformation is made to the system in Fig. 1-2, the new system is illustrated in Fig. 2-1,

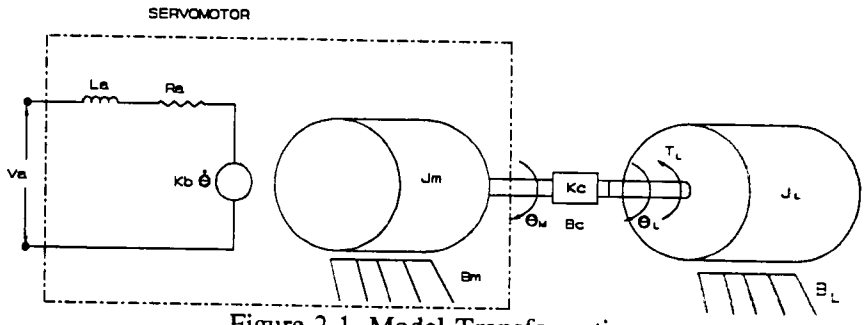


Figure 2-1, Model Transformation.

2-3. Derivation of the System Equations

By using Fig. 2-1, the mathematical equations describing the mechanical system can be written with the aid of free body diagrams. The diagrams are drawn by passing an imaginary plane through the center of the coupling and examining the action and reaction of both ends of the shaft. These diagrams are shown in Fig. 2-2 .

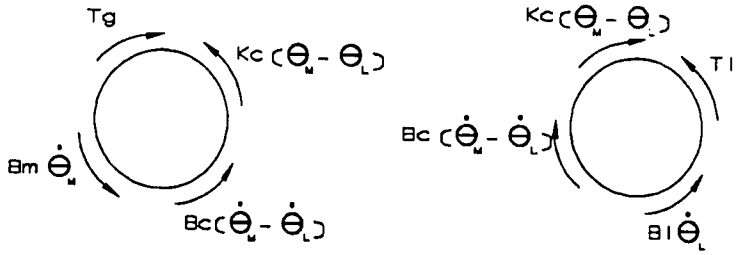


Figure 2-2, Free body diagrams.

Using Fig. 2-2, and using clockwise positive as the convention, the equations governing the mechanical system can be written by employing Newton's law for rotational motion,

$$\sum T = J\,\alpha \qquad (2\text{-}2)$$

where,

T= torque opposing motion

J= inertia

α= angular acceleration

By examining motor inertia, motor generated torque, shaft compliance and viscous damping the following equation can be written by summing the torques and setting them equal to the inertia times the angular acceleration.

$$T_g - K_c (\theta_m - \theta_l) - B_m \dot{\theta}_m = J_m \ddot{\theta}_m \qquad (2\text{-}3)$$

Where in the British units,

T_g= torque generated by motor (Ft.-Lb.)

K_c= coefficient of stiffness (Ft.-Lb./ rad)

θ_m= motor shaft position (rad)

θ_l= leadscrew position (rad)

B_m= viscous damping coefficient of motor (Ft.-Lb/(rad/s))

Another equation may be written by applying the same principles to the load inertia.

$$K_c (\theta_m - \theta_l) - T_l - B_l \dot{\theta}_l = J_l \ddot{\theta}_l \qquad (2\text{-}4)$$

Where,

T_l = torque due to normal force on leadscrew threads

B_l = viscous damping of the load

The next equation used to derive the model is written from the electrical circuit of the servomotor. By applying Kirchoff's voltage law, the sum of the voltages in a loop is zero, a third equation can be written.

$$V_a - i_a R_a - L_a \frac{di_a}{dt} - K_b \dot{\theta}_m = 0 \qquad (2\text{-}5)$$

Where,

V_a = applied motor voltage (Volts)

i_a = armature current (Amps)

L_a = armature inductance (Henry)

R_a = armature resistance (ohms)

K_b = counter e.m.f. constant (V/(rad/s))

Equations (2-3), (2-4) and (2-5) can be combined with an equation from elementary d.c. machine theory which relates the generated torque of a d.c. motor to the current flowing through the armature circuit [4]. This relationship is given as Eq. (2-6)

$$T_g = K_t I_a \qquad (2\text{-}6)$$

Using equation (2-6), three differential equations can be written to describe the mechanical and electrical system. For illustrative purposes, the differential operator will replace the dot notation in the previous equations; thus, equations (2-3), (2-4), (2-5) and (2-6) become.

$$K_t i_a - K_c(\theta_m - \theta_l) - B_m \frac{d\theta_m}{dt} = J_m \frac{d^2\theta_m}{dt^2} \tag{2-7}$$

$$K_c(\theta_m - \theta_l) - T_l - B_l \frac{d\theta_l}{dt} = J_l \frac{d^2\theta_l}{dt^2} \tag{2-8}$$

$$V_a - i_a R_a - L_a \frac{di}{dt} - K_b \frac{d\theta_m}{dt} = 0 \tag{2-9}$$

These three equations describe the physical dynamics of the motor, leadscrew and toolholder.

2-4 Derivation of the State Equations

In order to simulate the system and account for the non-linearity, the software program PCSIMNON was chosen. PCSIMNON is a very flexible software program which

enables the user to simulate any type of system in which the algebraic and/or differential equations can be written. Another advantage of PCSIMNON is its ability to interface with PCMATLAB which is a well known control system design tool for classical as well as modern control. The language allows the control system designer to write simple algebraic expressions to account for saturation, backlash and other non-linear quantities.

To utilize PCSIMNON the system equations must be placed in state variable form. Placing a set of nth order simultaneous differential equations into state variable form reduces the equations into a set of 1st order differential equations. The purpose of introducing the state variable approach enables the computer to solve the system with relative ease and speed. To transform the system equations into state variable form several algebraic substitutions must be made. Let,

$$X_1 = I_a = mc$$
$$X_2 = \dot{\theta}_m = msp$$
$$X_3 = \theta_m = mpos$$
$$X_4 = \dot{\theta}_l = lsv$$
$$X_5 = \theta_l = lsp$$

by taking the derivative of both sides of the above equations and substituting them into eqs. (2-3), (2-4) and (2-5) the system is transformed into the state variable form. The results are shown as eqs. (2-10) to (2-14).

$$\dot{X}_1 = \dot{I}_a = \left(\frac{1}{L_a}\right)\left(V_a - R_a X_1 - K_b X_2\right) \tag{2-10}$$

$$\dot{X}_2 = \ddot{\theta}_m = \left(\frac{1}{J_m}\right)\left(K_t X_1 - K_c (X_3 - X_5) - B_m X_2\right) \tag{2-11}$$

$$\dot{X}_3 = X_2 \tag{2-12}$$

$$\dot{X}_4 = \ddot{\theta} = \left(\frac{1}{J_l}\right)\left(K_c (X_3 - X_5) - T_l - B_l X_4\right) \tag{2-13}$$

$$\dot{X}_5 = X_4 \tag{2-14}$$

By substituting the descriptive variables into the above equations, the framework for the PCSIMNON simulation code can be written. To illustrate the signal flow in the open loop system, a simulation diagram has been constructed and is shown in Fig. 2-3. The simulation diagram shows all forward and feedback paths that exist in the system. The simulation diagram is used to develop the PCSIMNON simulation code.

$$dmc = \left(\frac{1}{L_a}\right)(V_a - R_a\ mc - K_b\ msp) \tag{2-14}$$

$$dmv = \left(\frac{1}{J_m}\right)(K_t\ mc - K_c\ (mpos - lsp) - B_m\ msp) \tag{2-15}$$

$$dlsp = msp \tag{2-16}$$

$$dlsv = \left(\frac{1}{J_l}\right)(K_c\ (mpos - lsp) - T_l - B_l\ lsv) \tag{2-17}$$

$$dlsp = lsv \tag{2-18}$$

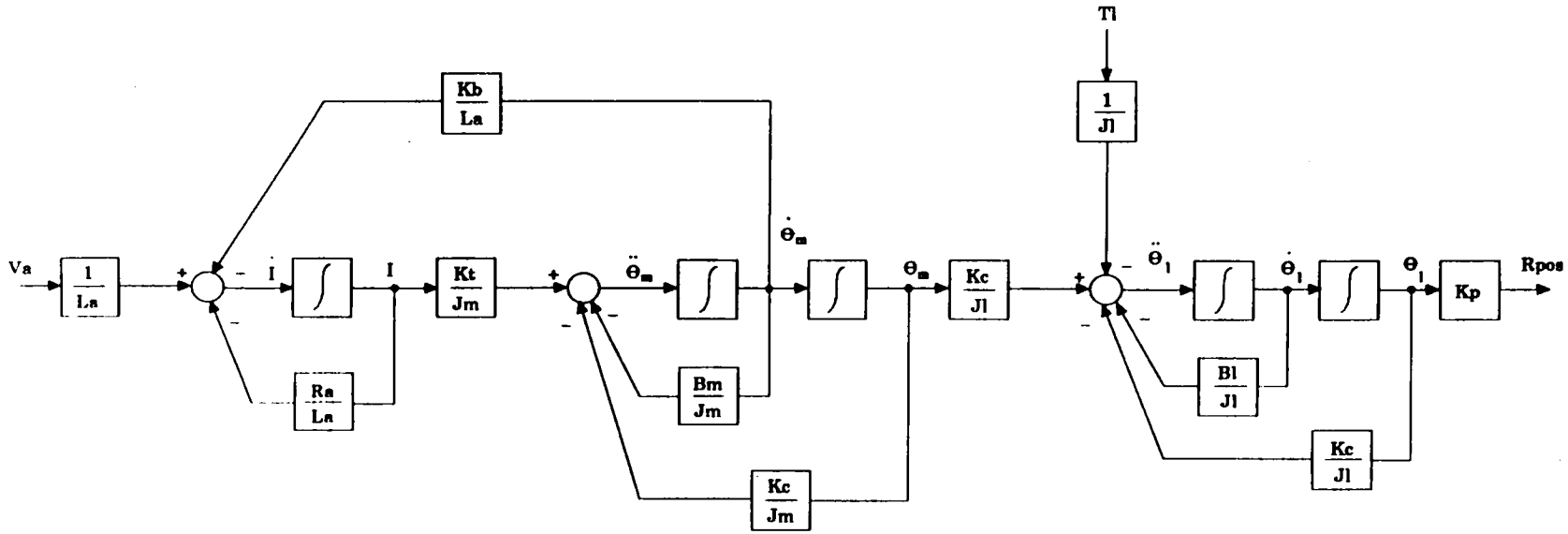


Figure 2-3, Simulation diagram.

2-5 The Laplace Domain Representation of the System

To utilize the analytical tools for classical control design and analysis the system is easiest represented by equations in the S-domain. The equations and subsequently the transfer function can be analyzed for response, stability and error. The system transforms into the S-domain, with the initial conditions set to zero, by replacing the differential operator by the S operator:

$$S^n = \frac{d^n}{dt^n} \tag{2-18}$$

this transformation allows a differential equation to be manipulated as an algebraic equation. By substituting eq. (2-18) into eqs. (2-7), (2-8) and (2-9) the following equations can be written,

$$K_t\, i_a - K_c\, \theta_m + K_c\, \theta_l - B_m\, S\, \theta_m = J_m\, S^2\, \theta_m \tag{2-19}$$

$$K_c\, \theta_m - K_c\, \theta_l - T_l - B_l\, S\, \theta_l = J_l\, S^2\, \theta_l \tag{2-20}$$

$$V_a - R_a\, i_a - S\, L_a\, i_a - K_b\, S\, \theta_m = 0 \tag{2-21}$$

2-6 Block Diagram Construction

To construct the block diagram that represents the system, eqs. (2-19, (2-20), and (2-21) are rewritten as:

$$\theta_m = \frac{K_t I_a - K_c \theta_l}{S^2 J_m + S B_m + K_c} \qquad (2\text{-}22)$$

$$\theta_l = \frac{K_c \theta_m - T_l}{S^2 J_l + S B_l + K_c} \qquad (2\text{-}23)$$

$$I_a = \frac{V_a - K_b S \theta_m}{S L_a + R_a} \qquad (2\text{-}24)$$

The block diagram that represents the system or plant is shown in Fig. 2-4, the block diagram gives an illustrative picture of the signal flow paths within the plant. The diagram reveals the built in feedback paths which exist within the plant. From the block diagram, the open loop transfer function can be derived by the use of Mason's gain formula and the principle of superposition. Since, there are two inputs to the system namely T_l and V_a the transfer function can be derived by first setting one of the inputs to zero and calculating the output to input ratio via Mason's gain formula. The process is completed by setting the other input variable to zero and calculating the output to input ratio then summing the responses to obtain the overall response. The above analysis is valid for linear systems, but as was previously mentioned the system described here is a non-linear system. To utilize the above analysis and analysis in the Laplace domain the system must be linearized.

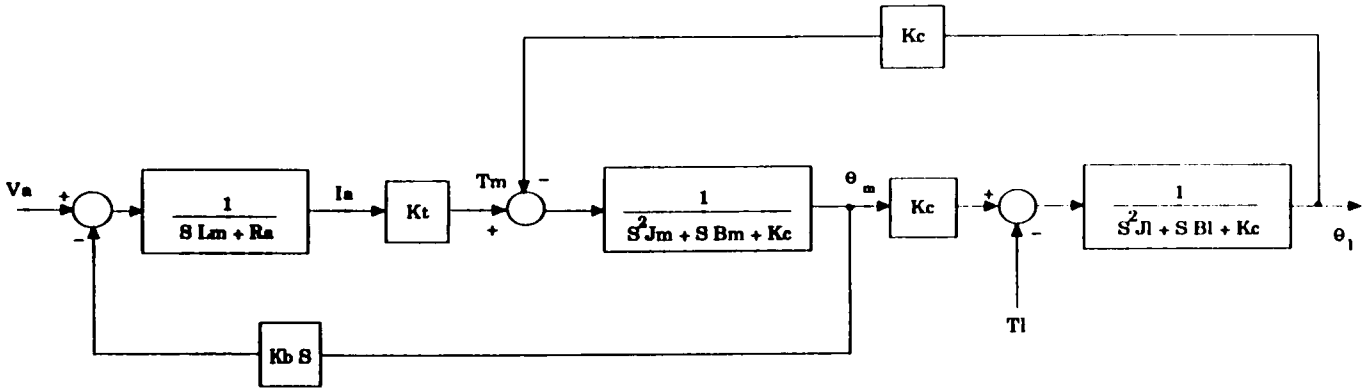


Figure 2-4, S-domain block diagram.

To linearize the system discussed here the torque required by the leadscrew must be considered to be constant over a specified range or set to zero. This assumption will be used in the design of the controller but, the simulation of the closed loop response will reflect the true dynamics of the system. Mason's gain formula is given by eq. (2-25),

$$T = \frac{\sum T_n \Delta_n}{\Delta} \qquad (2\text{-}25)$$

where T_n is the gain of the nth forward path and

$\Delta = 1 - \sum$ *of all individual loop gains*
$+(\sum$ *of gain products of all possible combinations of two nontouching loops)*
$-(\sum$ *of the gain products of all possible combinations of three nontouching loops)* $+ \cdots$

Δ_n = *the* Δ *for the part of the signal flow graph which is nontouching with the nth forward path*

The block diagram shown in fig. (2-4) will aid in the use of Mason's gain formula. To derive the transfer function of the leadscrew position with respect to the applied motor voltage the disturbance torque T_l will be set to zero. By examination there exists one forward path, thus:

$$T_1 = \frac{K_c K_t}{(S L_a + Ra)(S^2 J_m + S B_m + K_c)(S^2 J_l + S B_l + K_c)} \qquad (2\text{-}26)$$

Also, by examination there exists two minor gain loops, thus:

$$L_1 = \frac{-K_t K_b S}{(S L_m + R_a)(S^2 J_m + S B_m + K_c)} \qquad (2\text{-}27)$$

$$L_2 = \frac{K_c^2}{(S^2 J_m + S B_m + K_c)(S^2 J_l + S B_l + K_c)} \qquad (2\text{-}28)$$

By substituting eqs. (2-26), (2-27), and (2-28) into eq. (2-25) and simplifying, the open loop transmission from voltage applied to leadscrew position is found as:

$$\frac{\theta_l}{V_a} = \frac{K_t K_c}{S(A S^4 + B S^3 + C S^2 + D S + E)} \qquad (2\text{-}27)$$

where,

$$A = J_l J_m L_m$$
$$B = B_l J_m L_m + B_m J_l L_m + J_l J_m R_a$$
$$C = B_l (B_m L_m + J_m R_a) + B_m J_l R_a + J_l (K_b K_t + K_c L_m) + J_m K_c L_m$$
$$D = B_l (B_m R_a + K_b K_t + K_c L_m) + B_m K_c L_m + J_l K_c R_a + J_m K_c R_a$$
$$E = B_l K_c R_a + B_m K_c R_a + K_b K_c K_t$$

The open loop transmission from the load torque to the leadscrew position can be found by allowing the applied motor voltage to be zero and then applying Mason's gain formula as in the previous case.

The result is given as eq. (2-28).

$$\frac{\theta_l}{T_l} = \frac{N_3 S^3 + N_2 S^2 + N_1 S + N_0}{S (A S^4 + B S^3 + C S^2 + D S + E)} \qquad (2\text{-}28)$$

where,

$$N_3 = J_m L_m$$
$$N_2 = B_m L_m + J_m R_a$$
$$N_1 = B_m R_a + K_b K_t + K_c L_m$$
$$N_0 = K_c R_a$$

To calculate the output response as a function of the applied motor voltage and the load torque the principle of superposition is applied to eqs. (2-27) and (2-28). The leadscrew shaft position is given as a function of V_a and T_l in eq. (2-29).

$$\theta_l = \frac{V_a K_c K_t + T_l (N_3 S^3 + N_2 S^2 + N_1 S + N_0)}{S (A S^4 + B S^3 + C S^2 + D S + E)} \qquad (2\text{-}29)$$

2-7 Rotary to Linear Motion Transformation.

The motion of the toolholder moving along the slide is a linear motion; thus, a leadscrew is used to transform the rotary motion of the servomotor into the linear motion of the toolholder. To analyze the leadscrew it is necessary to know what type of screw thread, i.e. single or double thread, and the lead of the screw. The leadscrew used in this

analysis and in the mockup machine, is an ACME single thread type with an outside diameter of .5" and a thread lead of l= .16670 . To derive the constant of proportionality between the leadscrew shaft position and the toolholder position Eq. (2-30) will be used as will the fact that the pitch of a single ACME thread is equal to the lead of the screw.

$$l = p = .1667$$

$$y(\theta_l) = \frac{p\,\theta_l}{2\,\pi} \qquad (2\text{-}30)$$

$$y(\theta_l) = .0265\,\theta_l \qquad (2\text{-}31)$$

where,

p= pitch of the screw (inches/thread)

$y(\theta_l)$= tool holder position (inches)

The transfer function of the system has been defined in terms of the physical parameters of the system, these parameters must be defined or derived in order to produce a characteristic equation that can be examined analytically.

2-8 System Feedback

The ADM utilizes a laser interferometer to feedback the toolholder position to the controller via slip rings. The interferometer used is a Hewlett-Packard model 5100 with associated electronics to produce a signal proportional to the toolholder position. After inquiring with Hewlett-Packard as to the bandwidth of the inferometer, it was found to

be 2 Mhz. With this large bandwidth, a decision to model the interferometer as a unity gain system was made. With this assumption, the closed loop system is characterized by unity feedback from toolholder position to toolholder desired position. The complete system block diagram is shown Fig. 2-5; the gain block $G_c(S)$ represents the controller transfer function that is to be determined to give the desired surface finish.

2-9 System Parameters

The response of any dynamic system is a function of the system parameters. The system parameters dictate the coefficients of the S terms in the characteristic equation of the closed loop system which effectively defines where the poles of the system are located.

In order to obtain a transfer function which properly represents the system it is necessary to pay close attention to the system parameters whether they are given or derived. In the absence of a well defined transfer function, the poles of the characteristic equation may lie in the right half plane leading to an unstable system. Another situation which may arise is the variation of the plant parameters. These variations of the system may cause instabilities in the overall system response even though the characteristic equation was thought to be stable when analyzed.

In the ADM, many of the system parameters are governed by the servomotor that is used to move the leadscrew and ultimately the toolholder. These parameters have been characterized by the Inland Motor Company for the QT-5404 servomotor, the complete data sheet for this motor appears in the Appendix B. The salient parameters that will be

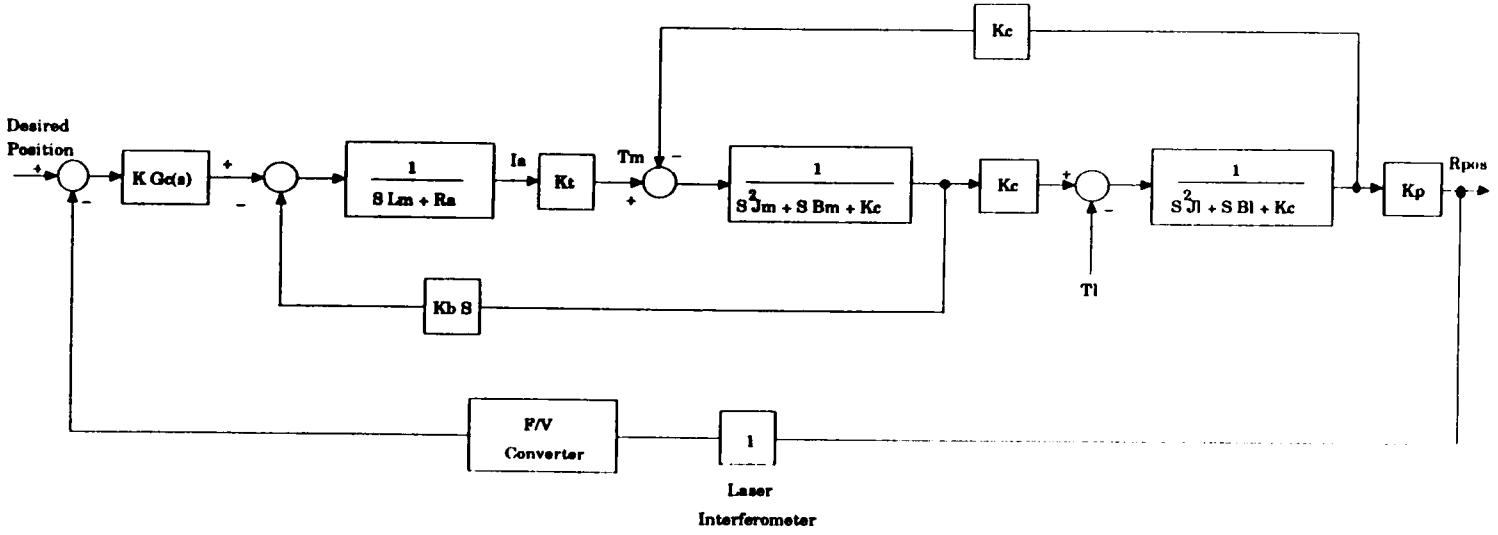


Figure 2-5, Complete block diagram.

utilized in the transfer function derivation, control design and simulation are listed in Table (2-1). The other parameters namely: J_l, T_l, B_l and K_c will be derived theoretically or found empirically from the mockup machine.

L_m= 3.6 mH (Armature Inductance)

R_a= 5 ohms (Armature Resistance)

J_m= 1.9E-3 Lb. Ft. S^2 (Armature Inertia)

B_m= .153 Lb. Ft./(rad/s) (Viscous damping of Motor)

K_t= .810 Lb. Ft./amp (Torque sensitivity)

K_b= 1.10 V/(rad/s) (Back EMF Constant)

W = 30-50 Lbs. (Tool Holder Weight)

d= .5 in. (Diameter of leadscrew shaft)

L= 78 in. (Length of leadscrew shaft)

Table 2-1, Known System Parameters.

a. Calculation of the Load Inertia

To calculate the inertia that is seen by the motor, it is necessary to consider the dynamics of the system past the coupling on the leadscrew side. The inertia seen by the motor is the sum of the inertia of the leadscrew itself and the transformed inertia of the tool holder mass. By using eq. (2-1), the transformed inertia can be calculated by substituting the required parameters.

Thus,

$$J_{th}=\frac{W}{g}\left(\frac{L}{2\pi}\right)^2$$

$$J_{th} = \frac{800}{386.4}\left(\frac{.1667}{2\pi}\right)^2 \qquad (2\text{-}1)$$

$$J_{th} = 1.46E\text{-}3 \quad (oz\text{-}in\text{-}s^2)$$

$$J_{th} = 7.59E\text{-}6 \quad (Ft\text{-}Lb.\text{-}s^2)$$

To calculate the moment of inertia of the leadscrew, the formula for the moment of inertia of a cylinder can be used as shown in [9]. The formula is given as eq. (2-32) .

$$J = \frac{\rho\ \pi}{2} R^4\ h \qquad (2\text{-}32)$$

Where,

ρ = density in weight per unit volume (oz./ in^3)

R = mean radius of the shaft (in.)

h = length of the shaft (in.)

Since a steel shaft will be used for the leadscrew, eq. (2-32) reduces to

$$J_{ls} = 0.0184\ h\ R^4 \quad oz\text{-}in.\text{-}s^2 \qquad (2\text{-}33)$$

By substituting the values of h and R, the value for the leadscrew shaft inertia can be calculated.

$$J_{ls} = 0.0184\ 78\ (.25)^4 \quad oz\text{-}in.\text{-}s^2$$
$$J_{ls} = 5.61E\text{-}3 \quad oz\text{-}in.\text{-}s^2$$
$$J_{ls} = 29.20E\text{-}6 \quad Lb.\text{-}Ft\text{-}s^2$$

Thus, the total inertia that will be connected to the coupling becomes:

$$J_l = J_{th} + J_{ls}$$
$$= 36.79E\text{-}6 \quad Lb.\text{-}Ft.s^2$$

b. Empirical Observation of the Load Viscous Damping B_l

The viscous damping coefficient was measured by instrumenting the mockup machine with a servomotor, tachometer and current probe. The motor was attached via a rigid coupling to the leadscrew shaft with the toolholder removed from the slide.

The motor was run at various speeds to generate a speed torque curve that revealed a slope of s=.0001. The curve was constructed by monitoring the current and speed, then using the torque constant of the motor to calculate the generated torque. The slope of the speed-torque curve represents the viscous damping coefficient B_l. Thus,

$$Bl = 0.0001 \quad Ft.\text{-}Lb/(rad/s)$$

c. Calculation of the Torsional Spring Constant

An attempt was made to measure the torsional spring constant K_c from the mockup machine, this proved to be quit a task and was abandoned after several attempts. To

calculate K_c an equation from mechanics can be used [4]. This equation is given as eq. (2-34).

$$K_c = \frac{\pi d^4 G}{384\ L} \quad \frac{Ft.\text{-}Lb.}{rad} \tag{2-34}$$

where,

G= shear modulus = 12E6 psi for Steel

d= diameter of the shaft (in.)

L= length of the shaft (in.)

By substituting the values into eq. (2-34), the torsional spring constant can be calculated as:

$$K_c = \frac{\pi\ (.5)^4\ 12E6}{384 \cdot 78} \quad \frac{Ft.\ Lb.}{rad}$$

$$K_c = 78.665 \quad \frac{Ft.\text{-}Lb.}{rad}$$

The last parameter necessary for the system is the expression for the load torque. The load torque will be considered as a disturbance input to the system as reflected in the block diagram. The calculation of this disturbance will be developed in the next section.

2-10 Derivation of Load Torque Expression

To derive an expression for the load torque it is necessary to examine the physics of the leadscrew, tool holder and rotating beam. This is accomplished by the use of free

body diagrams describing the tool holder and leadscrew. The free body diagram for the tool holder including all associated forces is shown in Fig. 2-6 .

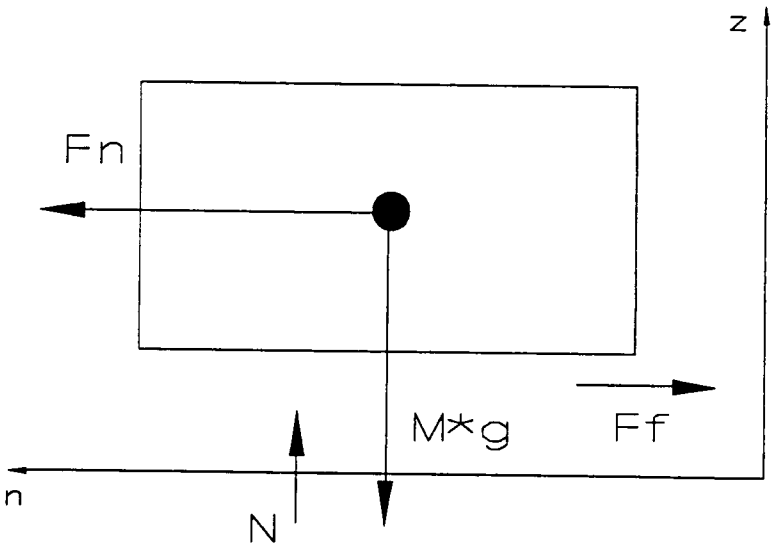


Figure 2-6, Free Body Diagram of Tool Holder.

By assuming that the tool holder is supported by frictionless air bearings, the following equations can be written from the free body diagram:

$$F_n - F_f = \frac{V^2 M}{r}$$

$$F_f = 0$$

$$F_n = \frac{V^2 M}{r} \qquad (2\text{-}35)$$

Where,

F_n = *Normal force on leadscrew*

M = *mass of the toolholder*

r = *radius* =y (θ_i)

V = *Tangential velocity*

The mass of the toolholder will remain constant but the tangential velocity will change as a function of the radius. By substituting $V = \omega_m r$ and $M = W/g$, eq. (2-35) can be written as:

$$F_n = \frac{(\omega_m r)^2 W}{r g}$$

$$F_n = \frac{\omega_m^2 r W}{g}) \qquad (2\text{-}36)$$

The final expression for the normal force is derived by substituting the numerical values for ω_m and M. Since the rotating beam rotates at 100 rpm, the radian speed is found by unit conversion to be 10.47 rad/s. The value for the mass M of the slide can be calculated by using M= W/g where g is the gravitational force; therefore, the mass of the toolholder M= 1.55 lb. . By substitution into eq. (2-36) the normal force as a function of the radius is given as eq. (2-37)

$$F_n = 169.98 \cdot r \qquad (2\text{-}37)$$

The normal force acting upon the leadscrew threads will result in the load torque that must be overcome in order to move the toolholder. To continue with the analysis, it is necessary to examine the normal force acting upon the leadscrew threads, an assumption has been made that the normal force acting upon the threads is centered on the thread face. By examining the free body diagram in Fig. 2-7 an expression for the load torque can be derived.

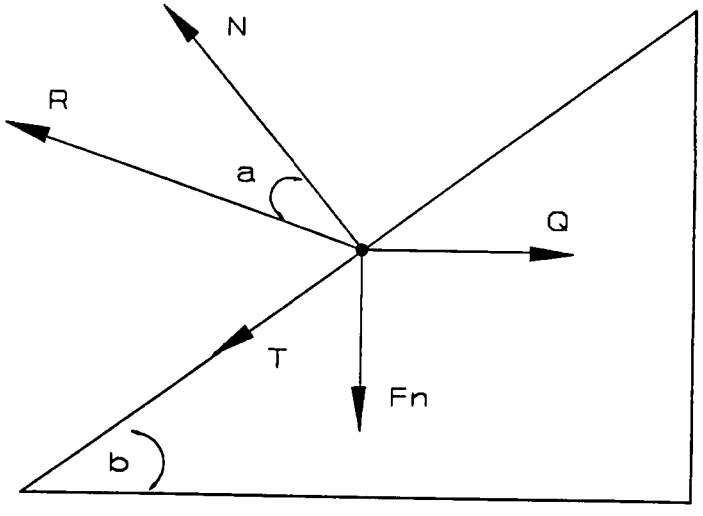


Figure 2-7, Leadscrew thread analysis.

The equations for the angles are:

$$TAN\ a = \frac{T}{N} = f \qquad (2\text{-}38)$$

$$TAN\ b = \frac{screw\ lead}{\pi\ D_m} \qquad (2\text{-}39)$$

The equations for the forces are written as eqs. (2-40) through (2-43):

$$Q = R\ SIN\ (a + b) \quad (2\text{-}40)$$

$$F_n = R\ COS\ (a+b) \quad (2\text{-}41)$$

$$\frac{Q}{F_n} = \frac{R\ SIN\ (a+b)}{R\ COS\ (a + b)} \quad (2\text{-}42)$$

$$Q = F_n\ TAN\ (a + b) \quad (2\text{-}43)$$

By multiplying both sides of eq. (2-43) by the mean radius an torque expression can be written as eq. (2-44).

$$\frac{Q\ D_m}{2} = \frac{F_n\ D_m}{2}\ TAN\ (a + b) = Torque = T_l \quad (2\text{-}44)$$

By utilizing a trigonometric identity for the tangent of the sum of to angles, eq. (2-45) can be written for the load torque.

$$T_l = \frac{F_n\ D_m\ [\ TAN\ b + TAN\ a\ ]}{2\ (\ 1 - f\ TAN\ b)} \quad (2\text{-}45)$$

Where,

f = coefficient of friction

Dm = mean diameter of leadscrew shaft

The expression for the load torque as a function of the radius of the toolholder can be written by substituting the values for Fn, Dm, and TAN b . The load torque as a function of the coefficient of friction and the radius is given as eq. (2-46).

By deriving equation (2-46), a graph of the load torque versus radius is shown in Fig.(2-8), the value of the friction coefficient f was chosen to be .001 based on leadscrew data [10].

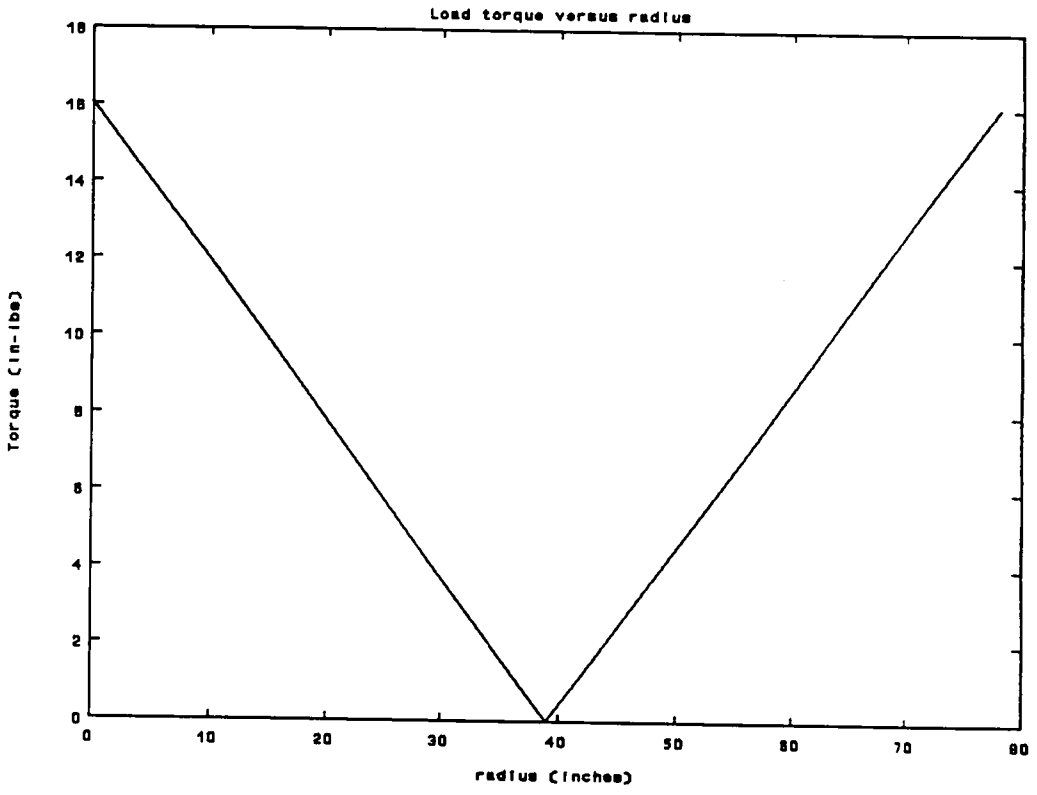


Figure 2-8, Load torque.

$$D_m=\frac{Od-Id}{2}=\frac{.5+.475}{2}=.488$$

$$Tan\ b=\frac{.1667}{\pi \cdot .488}=.109$$

$$Tan\ b=.001$$

$$F_n=169.98 \cdot r$$

$$T_l(r,f)=\frac{41.48 \cdot r \cdot (.109+f)}{(1-.109 \cdot f)} \qquad (2\text{-}46)$$

The graph's V shape is due to normal force F_n becoming zero at L/2, L is the leadscrew length, by examination of eq. (2-45) it can be seen that the torque also becomes zero.

To perform the S-domain analytical study of the plant, the system parameters are substituted into eq. (2-29) yielding a transfer function that describes the response of the

leadscrew shaft due to the driving function $V_a(s)$ and the disturbance torque $T_l(s)$. By substituting eq. (2-31) into eq. (2-29), the plant transfer function $G_p(s)$ represents the position of the actual tool holder due to the driving function $V_a(s)$.

Generally, the classical control method is best used for analysis and synthesis of SISO (single input single output) systems. By setting the disturbance torque $T_l(s)=0$ in eq. (2-29), the equation is simplified to represent a SISO system. By reducing the transfer function to a SISO system the controller can be designed using classical control theory to meet the performance specifications. The next chapter describes the analysis of the plant transfer function $G_p(s)$ and the synthesis of the controller $G_c(s)$. The plant transfer function $G_p(s)$ is given below as eq. (2-47).

$$\frac{5.6E8}{S\,(S^4 + 1472\,S^3 + 2426E3\,S^2 + 3200E6\,S + 5178E8)} \qquad (2\text{-}47)$$

CHAPTER 3

CONTROL OF THE DYNAMIC SYSTEM

3-1 Introduction

The control study begins with defining or having specified the relevant performance specifications that must be met. Once the specifications are known, the control engineer must decide on which type of control would be best, given the performance criteria. In classical control there are several types of control schemes: PID, phase lag, phase lead, lead-lag, feedback control, etc. . All of these control schemes have their own merits from which the designer can choose. The classical control method is generally applicable to most low to medium performance systems; the major limitation in classical control is its inability to formally handle multiple input single output (MISO) and multiple input multiple output (MIMO) systems.

Modern control system theory presents the design engineer with a unified method of control to achieve the desired closed loop response of SISO, MISO and MIMO systems. In utilizing modern control theory, the dynamic system is described by a set of first order differential state equations. These equations are placed in vector and matrix form for analysis and design. One major advantage of modern control over classical control is the availability to examine various states within the dynamic system or plant. In many cases, there are oscillations and instabilities within the plant that are not revealed by the S domain transfer function representing $G_p(s)$. For example, a servomotor represented in the state variable form would most likely have the armature current I_a as a state variable.

Simulation by a program such as MATLAB or SIMNON may reveal an oscillation in I_a that would cause eddy currents to flow in the pole pieces, thus, causing excessive heating and eventual destruction of the servomotor.

In this chapter, the performance specifications of the dynamics of the open loop system as well as the closed loop system will be explored in order to reveal deficiencies in meeting the criteria without some type of compensation. Then, two different approaches will be performed to compensate the system to meet the desired performance specifications.

3-2 Specifications

The specifications given to the control design engineer provide a basis for choosing the proper type of compensation. In most cases, the specifications are well defined but in experimental machines the specifications may be unknown or vague. For the ADM, there were no given specifications other than the desired surface finish of 1 inch. The mock-machine was also unavailable for inspection due to its location in a classified area at Y-12. In order to proceed with a control design, certain specifications will be defined by using previous experience and rules of thumb.

Since the system described in this thesis is a machining operation, experience dictates that the steady state error should be as small as possible if not zero. The control signal chosen for this system is a ramp function which lends itself well to controlling a machining operation. The step function will be used only as a test signal to explore the speed of response of the system. In practice, the step function for this system is not

relevant except in cases where it is desired to position the tool before starting to make any cuts on the material. Once the cutting operation has begun, the ramp function provides a smooth and precise way to position the tool holder to achieve the desired surface finish. The following table describes the design specifications that will be used as the criteria to design the control system.

Closed loop design specifications

Surface finish= $e_{ss} < 1\ \mu$ inch

Overshoot < 20%

Settling time < 400 mS

3-3 Error Analysis

To examine the performance of the closed loop system, a mathematical expression of the steady state error will be derived. The following diagram Fig. (3-1), describes the closed loop unity feedback case.

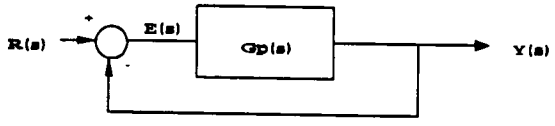


Figure 3-1, Block diagram of closed loop system.

By examination of fig.(3-1), the following equation for the error E(s) can be written:

$$E(s) = \frac{R(s)}{1 + G_p(s)} \qquad (3\text{-}1)$$

a substitution for $G_p(s)$ can be made by setting,

$$G_p(s) = \frac{K_p \prod (s-z_i)}{\prod (s-p_i)} \qquad (3\text{-}2)$$

for an all pole system with a pole at the origin $G_p(s)$ becomes.

$$G_p(s) = \frac{K_p}{s \prod (s-p_i)} \qquad (3\text{-}3)$$

By substituting eq.(3-3) into eq.(3-1) and performing some algebra eq.(3-1) becomes:

$$E(s) = \frac{R(s)\ s \prod (s+p_i)}{s \prod (s+p_i) + K_p} \qquad (3\text{-}4)$$

Using the final value theorem from Laplace transform theory, the steady state error in the time domain can be written as eq. (3-5),

$$e_{ss} = \lim_{s \to 0} [s\ E(s)] \qquad (3\text{-}5)$$

for a step function R(s)=1/s eq. (3-5) becomes,

$$e_{ss} = \lim_{s \to 0} \left(s \frac{1}{s} \frac{s \prod (s+p_i)}{s \prod (s+p_i) + K_p} \right) \qquad (3\text{-}6)$$

By taking the limit of eq. (3-6), the steady state error reduces to:

$$e_{ss} = \frac{0}{K_p} = 0$$

The above result shows that for a system with at least one pole at the origin, the steady state error is zero in response to a step function. The steady state error due to a ramp

function will be examined to provide the necessary information to choose a particular control strategy. Consider the ramp function input:

$$R(s) = \frac{1}{s^2}$$

Equation (3-5) becomes,

$$e_{ss} = \lim_{s \to 0} \left(s \frac{1}{s^2} \frac{s \prod (s+p_i)}{s \prod (s+p_i) + K_p} \right) \tag{3-7}$$

By taking the limit, eq. (3-7) reduces to,

$$e_{ss} = \frac{\prod p_i}{K_p} \tag{3-8}$$

As can be seen by eq.(3-7), another pole at the origin must be present in order for the system to have a zero steady state error or a very large gain to produce a small steady state error. Since the required gain is very large, a lag controller will be used. The lag controller has the following transfer function:

$$G_c(s) = K_c \frac{(s+z)}{(s+p)} \tag{3-9}$$

Where, p << z . If the same error analysis used above is performed using the cascade controller, the steady state error becomes:

$$e_{ss} = \frac{p_c \prod p_i}{K_p K_c z_c} \tag{3-10}$$

By using the necessary condition, p << z the above equation reveals a decrease in the steady state error by a factor of:

$$\frac{p_c}{K_c\ z_c}$$

The results of the steady state error analysis will be used to verify the choices for p_c, z_c and K_p. This will allow a quantitative measure of the performance of the controller with regards to meeting the error requirement that was described in section (3-2). The next section will describe the steps necessary to design the lag controller.

3-4 Closed loop response

In order to gain some insight into the required controller action, a simulation of the closed loop system with gain only (K_c=100e3) is shown in Fig. (3-1) for a step input and Fig. (3-2) for a ramp input. As can be seen in Fig. (3-2), there exists considerable error in the tracking response to the ramp function input signal.

The magnitude of the steady state error is calculated by using a modified eq. (3-8) and the roots of $G_p(s)$ in eq. (2-47). The roots of the denominator of eq. (2-47) can be found using the root solving macro in MATLAB, and are found to be:

$$\begin{aligned} s_1 &= 185.3 \\ s_2 &= 1282 \\ s_{3,4} &= 2.6 \pm j\ 1477 \end{aligned} \qquad (3\text{-}11)$$

The modified steady state error equation is:

$$e_{ss} = \frac{\prod p_i}{K_p K_c} \qquad (3\text{-}12)$$

One will note that the pole at the origin was accounted for in the derivation of eq. (3-8). By substituting the proper values in eq. (3-12) the steady state error is:

$$e_{ss} = \frac{(185.3)\ (1282)\ (2.6^2 + 1477^2)}{(5.6E8)\ (100E3)} = .00925$$

The above result correlates with the error shown in Fig. (3-2), and shows that the error requirement set forth in section 3-2 cannot be met by using a gain only controller. The next section shows how the root locus is reshaped to provide the desired response and meet the error requirement.

3-5 Controller Design

The design of the lag controller begins by deciding where on root locus the dominant poles will reside. The response of the system can be approximated by a second order transfer function for purposes of designing the controller, after a controller is designed the full order system is simulated and the parameters of the cascade filter are adjusted to yield the desired response. The response of the second order system has been studied in various references, the design equations used here will not be derived but may be found in [6]. The second order polynomial may characterized by the following:

$$P(s) = s^2 + 2\,\zeta\,\omega_n\,s + \omega_n^2 \qquad (3\text{-}13)$$

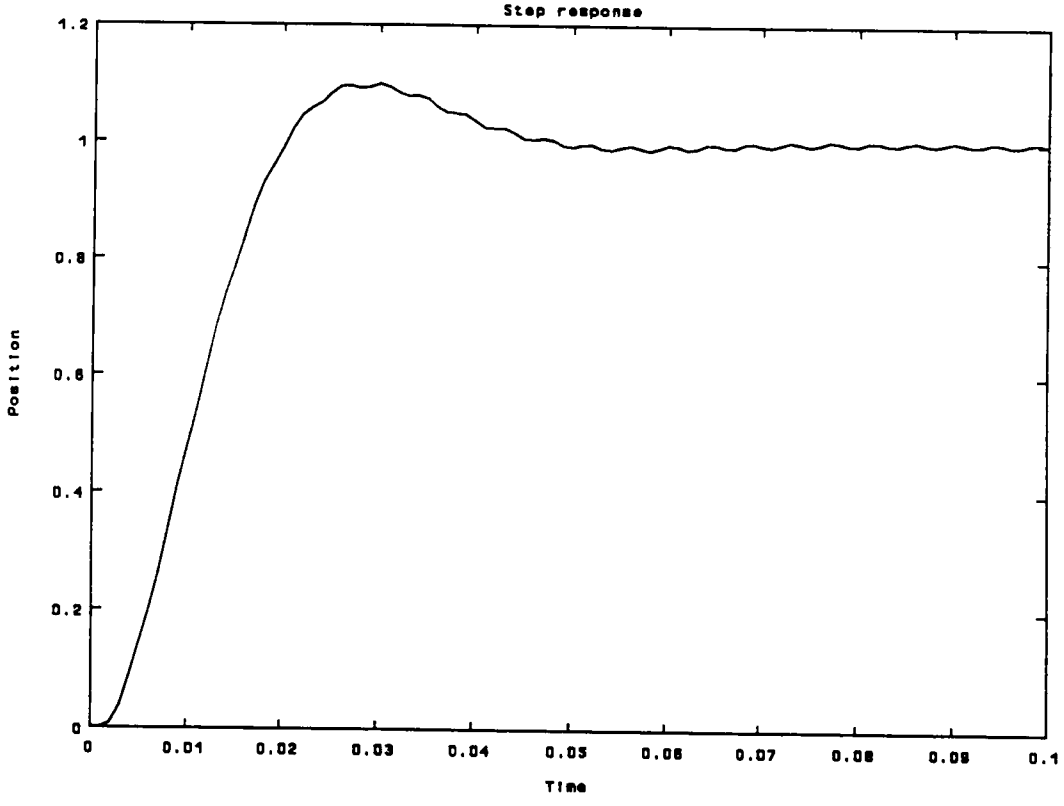


Figure 3-2,
Step response of system with gain added.

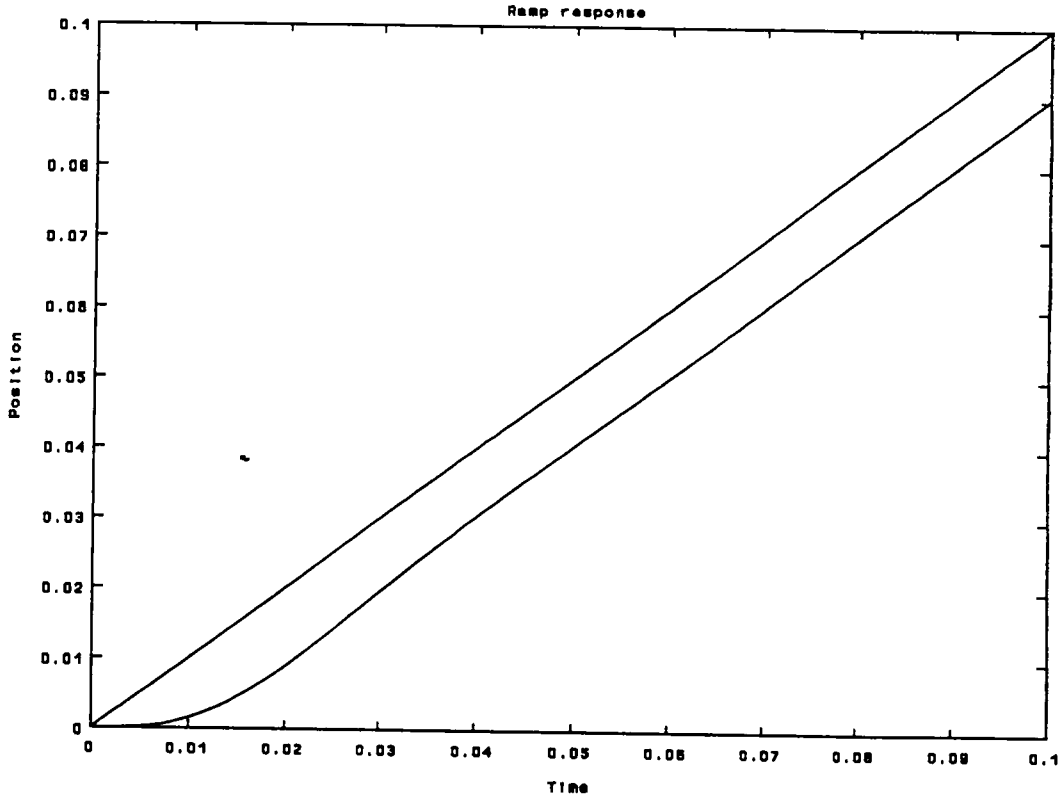


Figure 3-3,
Ramp response of system with gain added.

The above equation in the s-domain corresponds to the following in the time domain:

$$t_s = \frac{4.6}{\sigma}$$

$$t_r = \frac{1.8}{\omega_n}$$

$$\sigma = \zeta\ \omega_n$$

$$\omega_d = \omega_n \sqrt{1-\zeta^2}$$

$$M_p = 15\% \ , \ \zeta = 0.5$$

Where,

$$\sigma = \Re \textit{ part of the } P(s)$$

$$\omega_d = \Im \textit{ part of } P(s)$$

$$\zeta = \textit{Damping coefficient}$$

$$t_s = \textit{settling time}$$

$$t_r = \textit{rise time}$$

$$M_p = \textit{overshoot}$$

The equations above will be used to provide a basis for the location of the dominant poles on the root locus. Let the desired parameters be:

$$\zeta = .5$$

$$t_r = .03s$$

Then by substitution,

$$\omega_n \approx \frac{1.8}{t_r} = \frac{1.8}{.03} = 60$$

$$\sigma = \zeta\ \omega_n = (.05)\ (60) = 30$$

$$\omega_d = \omega_n \sqrt{1-(.5)^2} = 52$$

By letting p=.01 in equation (3-9), and using the angle and gain condition for the root locus the value of z can be found so that the root locus passes through the desired closed loop poles. The angle and gain condition is found in [6], and is given as:

$$\angle G = (2\,n + 1)\,180^\circ \;,\; n = \textit{any integer} \tag{3-14}$$

$$K = \frac{1}{|G|} \tag{3-15}$$

The angle of the controller zero can be found by re-writing equation (3-14) and measuring the angles from the pole-zero plot shown in Fig.(3-3). Eq (3-14) becomes:

$$\sum \angle z - \sum \angle p = (2\,n + 1)\,180^\circ$$

$$\angle z_c - \sum \angle p = -540^\circ \;,\; n = -2$$

$$\angle z_c = \sum \angle p - 540^\circ$$

From the pole-zero plot,

$$\sum \angle p = 620.8^\circ \;,\; \textit{then}$$

$$\angle z_c = 620.8^\circ - 540^\circ$$

$$\angle z_c = 80.8^\circ$$

In order to find the point on the real axis to place the zero, the following equation can be written:

$$\tan\angle z_c = \frac{\omega_d}{z_c - \sigma} \tag{3-16}$$

Solving for the controller zero eq.(3-16) becomes:

$$z_c = \frac{\omega_d}{\tan \angle z_c} + \sigma$$

$$z_c = \frac{52}{\tan 80.8} + 30 \qquad (3\text{-}17)$$

$$z_c = 38.42$$

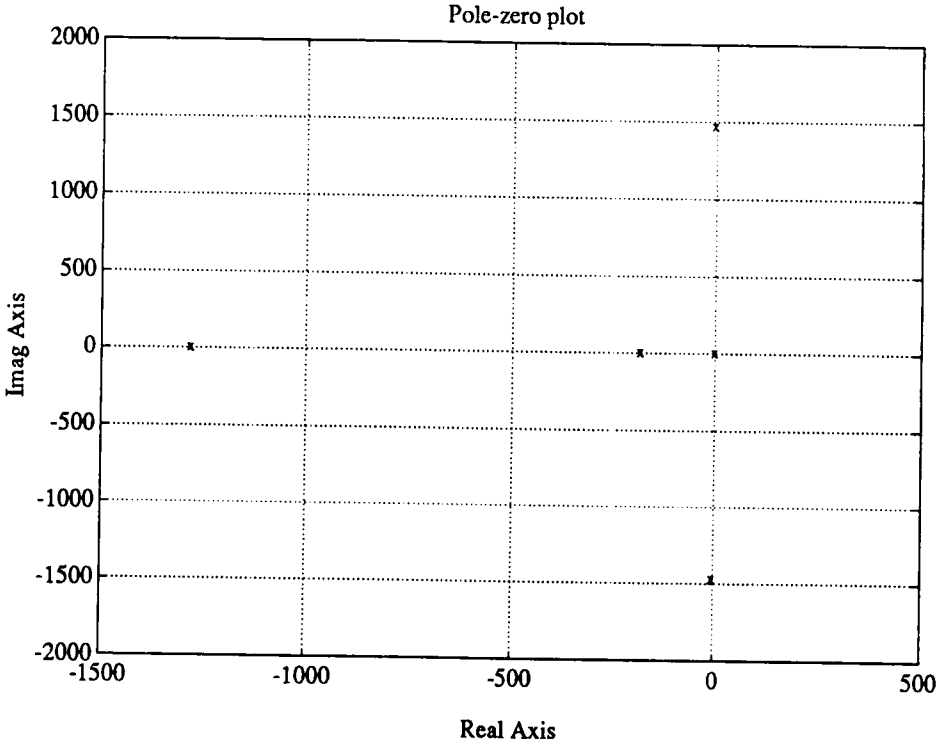


Figure 3-4, Pole-zero plot.

The magnitude of K is found by measuring the vector lengths from each pole and zero to the closed loop pole location, K is expressed as:

$$K = \frac{(1225)\ (1635)\ (1370)\ (75)\ (75)\ (180)}{(53)}$$

$$K = 52.4E{+}12$$

Since $K=K_p\ K_c$, K_c becomes;

$$K_c = \frac{K}{K_p} = \frac{52.4E{+}12}{5.6E{+}8} = 93.6E{+}3$$

Thus, the first try at a suitable controller is:

$$G_c(s) = 93.6E3\ \frac{(s\ +\ 38.4)}{(s\ +\ .01)}$$

By using eq. (3-10) and the result of eq. (3-12), the steady state error with the cascade controller implemented becomes:

$$e_{ss} = (.00925)\ \frac{p_c}{K_c\ z_c} = (.00925)\frac{.01}{(93.6E3)\ (38.4)} = 25.7E{-}12$$

The value of the steady state error is now well within the specification defined in section 3-2 ; furthermore, there exists enough latitude in the error such that minor changes in the controller parameters will still allow the error to be within the desired band.

3-6 Effect of Control on Root Locus

Figures 3-4 and 3-5, show the root locus for both the uncompensated system and the compensated system. As can be seen, the root locus of the compensated system has moved the roots of the characteristic equation towards the more stable region of the S plane.

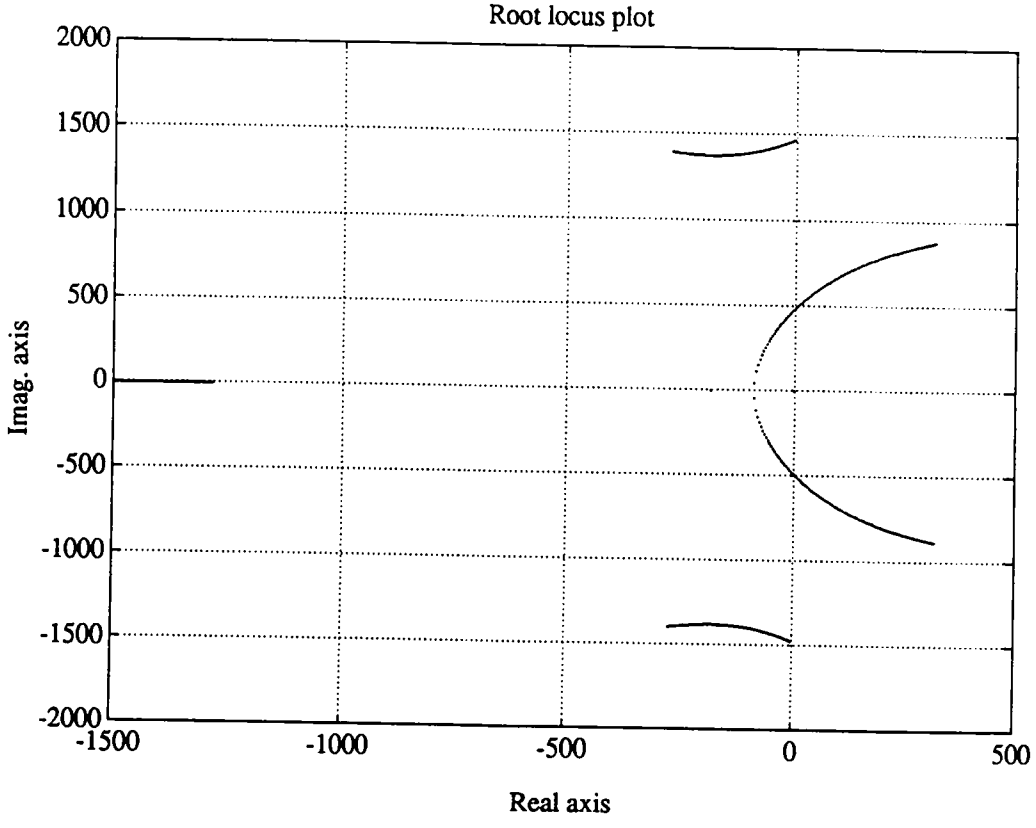


Figure 3-5, Uncompensated root locus.

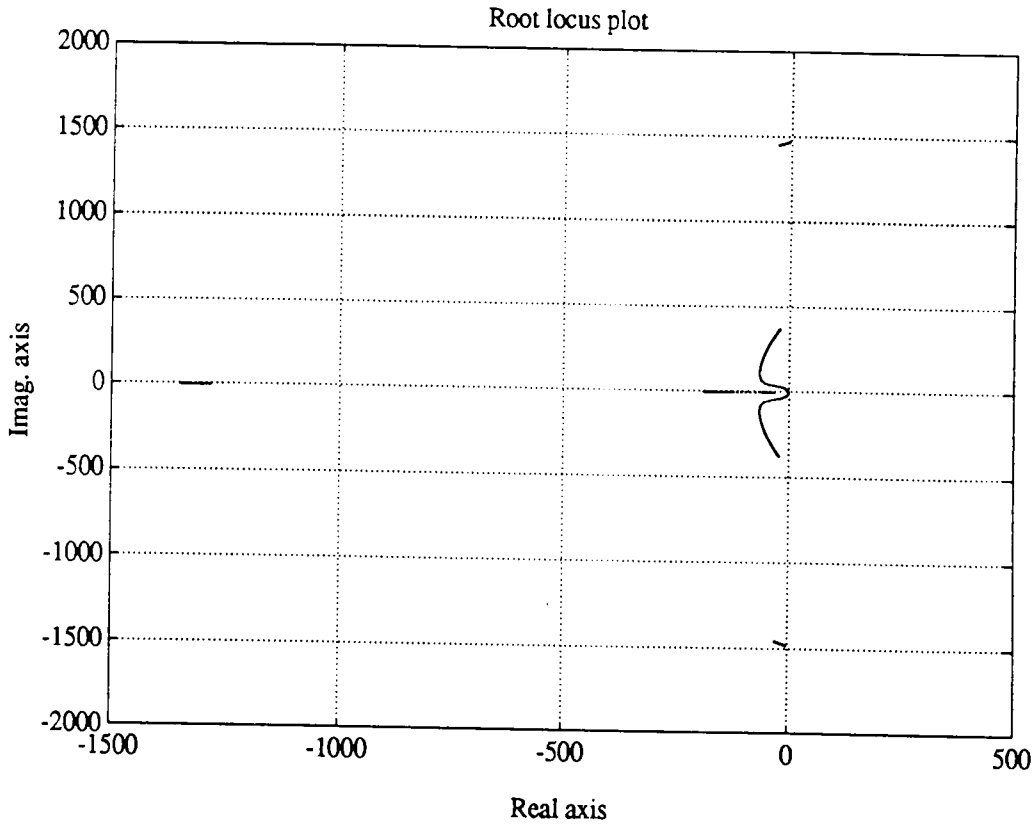


Figure 3-6, Compensated root locus.

In the next chapter, the controller will be simulated using SIMNON to reveal any deficiencies in meeting the specifications. At this point, the parameters of the controller will be adjusted so as to provide the best closed loop response for both a ramp and a step function.

CHAPTER 4

SYSTEM SIMULATION

4-1 Overview

To simulate the controller design of chapter 3, PCSIMNON was chosen because of the flexibility that the program offers. The first simulation was done to verify the controller design, the results revealed that the overshoot was unacceptable. To reduce the overshoot it was necessary to move the controller zero toward the right half plane and reduce the controller gain. The new controller transfer function is:

$$G_c(s) = 85E3 \frac{(s + 30)}{(s + .01)} \tag{4-1}$$

The results of the simulation of the above controller are shown in Figures 4-1 and 4-2. Figure 4-3 and 4-4 show the effect of the controller on the steady state error due to a ramp input. The error is minimized by the addition of the pole close to the origin, this pole provides a pseudo integral control. The steady state error is now within specifications if the system is considered to be linear, the next chapter will reveal the profound effect of adding the load torque, backlash and saturation.

4-2 Practical implementation of cascade controller

The transfer function given in eq. (4-1), can be implemented using three operational amplifiers and 10 passive devices. The transfer function of the first amplifier of the controller is given as eq. (4-2).

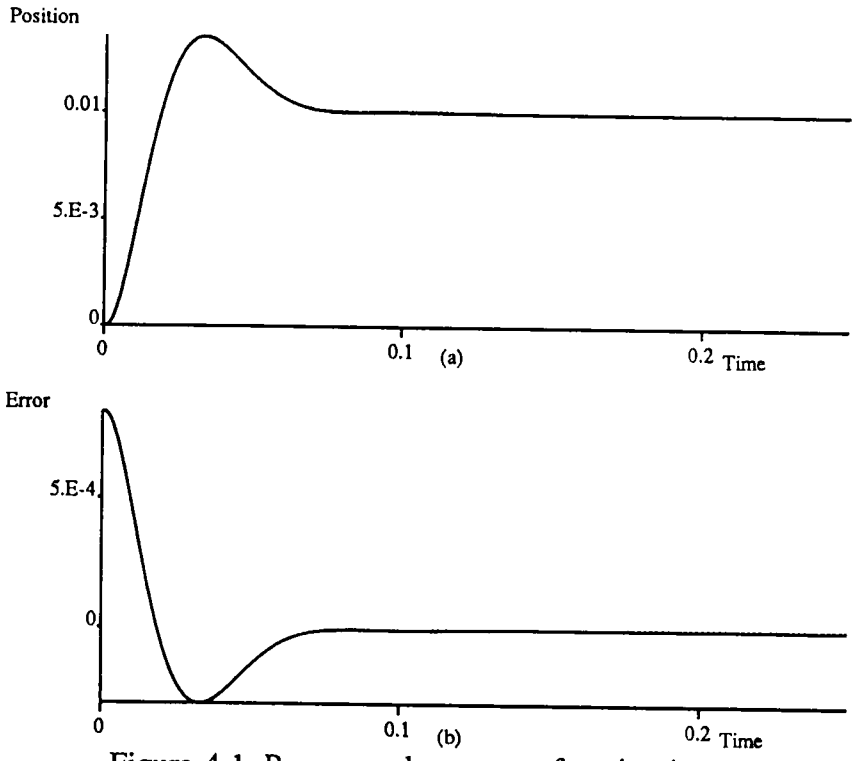


Figure 4-1, Response due to step function input:
(a) Position response, (b) Error response.

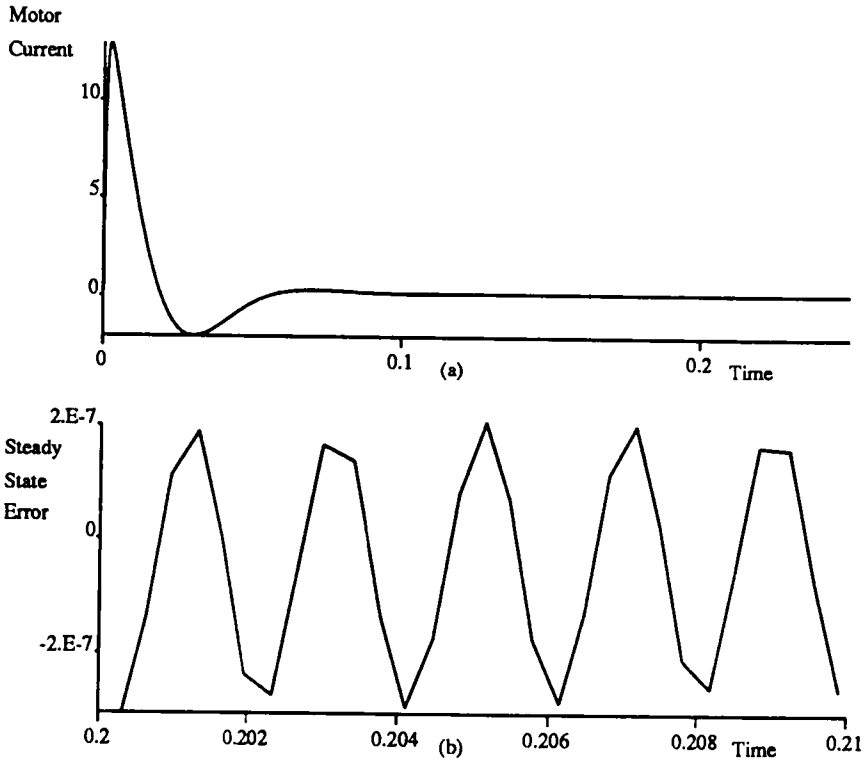


Figure 4-2, Response due to step function input:
(a) Motor Current, (b) Steady State error.

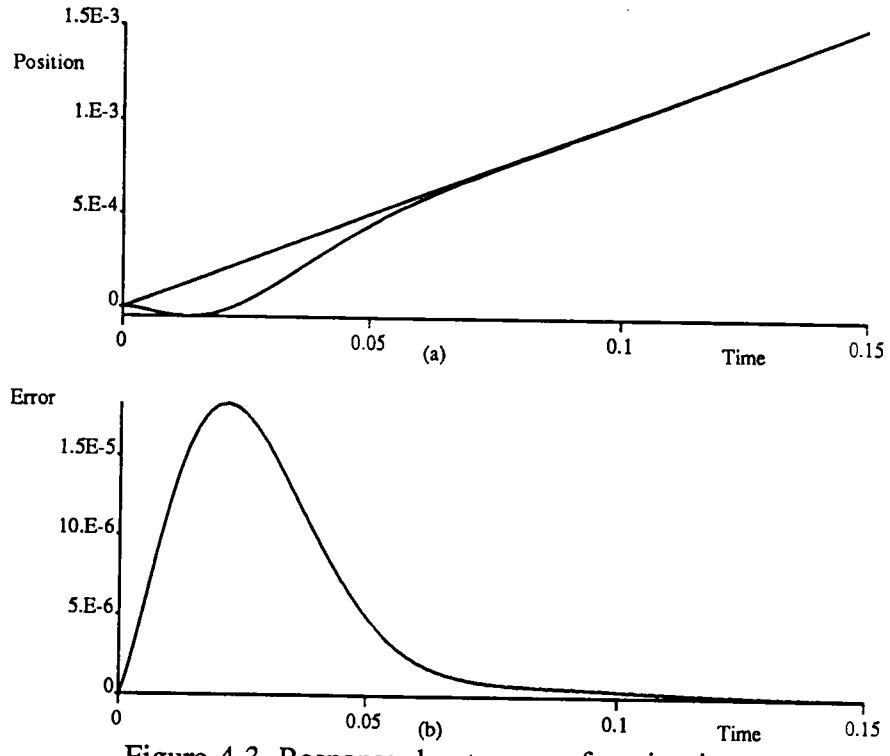


Figure 4-3, Response due to ramp function input:
(a) Position response, (b) Error response.

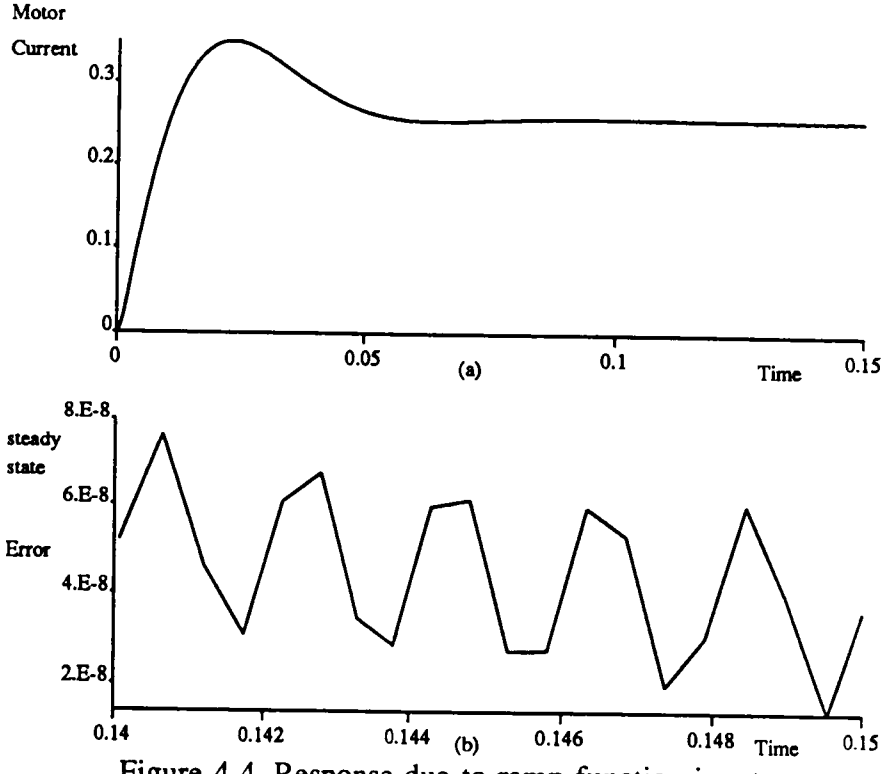


Figure 4-4, Response due to ramp function input:
(a) Motor current, (b) Steady State error.

$$T(s) = \frac{R_4}{R_2}\frac{\left(s + \frac{1}{\alpha T}\right)}{\left(s + \frac{1}{T}\right)} \qquad (4\text{-}2)$$

Where,

$$\alpha = \frac{R_4}{R_3 + R_4} \qquad (4\text{-}3)$$

$$T = R_3 C_1 \qquad (4\text{-}4)$$

Since T=100 then,

$$\alpha = \frac{1}{(30)(100)} = 333E\text{-}6$$

$$R_3 = R_4 \frac{1 - \alpha}{\alpha}$$

If R_4 =510 Ω 1% then,

$$R_3 = (510)\frac{(1 - (333E\text{-}6))}{(333E\text{-}6)} = 1.5\ M\Omega$$

$$C_1 = \frac{(100)}{(1.5E6)} = 68\ \mu F$$

And if the D.C. gain is set to 10, the following can be written:

$$R_2 = \frac{R_4}{(10)} = \frac{(510)}{(10)} = 51\Omega$$

In order to achieve the proper gain constant for the controller transfer function, two additional gain stages must be added, one being inverting and the other non-inverting. The gain constant is set to A_v=85E3, the first amplifier has a gain constant of 10; therefore, the two stages must provide a gain of 8500. If the gain is equally distributed between both amplifiers, each amplifier will require a gain of 92. Due to the simplicity of the second and third stages, the calculation of the resistor values will not be shown. The complete compensator schematic with the appropriate values is shown in Fig.(4-5).

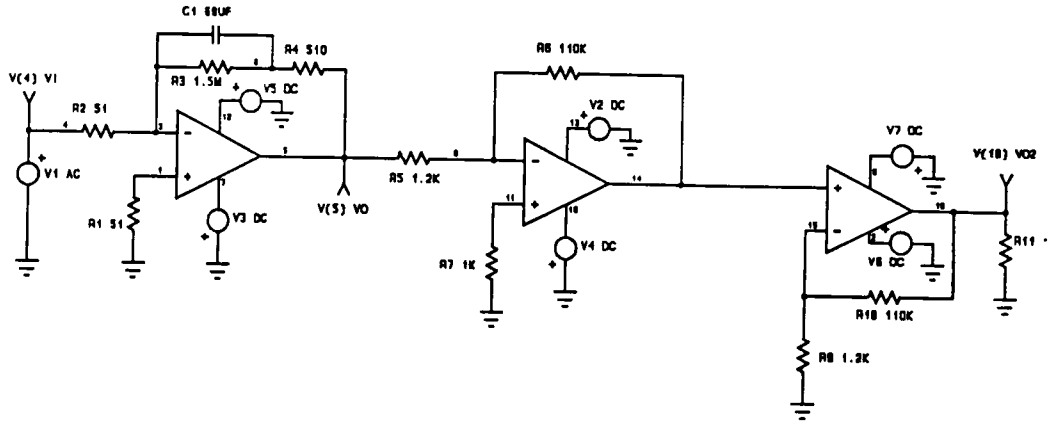


Figure 4-5, Practical implementation of controller.

A SPICE simulation was performed to verify the values calculated for the compensator, the Bode plot is shown in Fig. (4-6) and Fig. (4-7). As can be verified, the high frequency gain is 98.6 dB which corresponds to a gain of 85E3. The next chapter will explore the effects of perturbations on the linear system, suggestions will be made so as to minimize these effects before the machine is built.

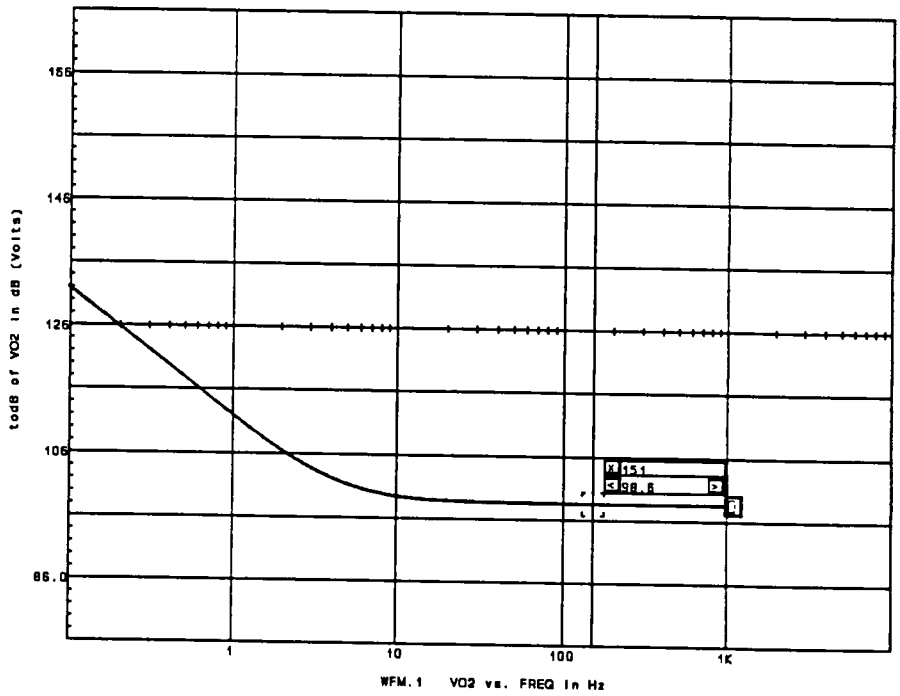


Figure 4-6, Gain plot of controller transfer function.

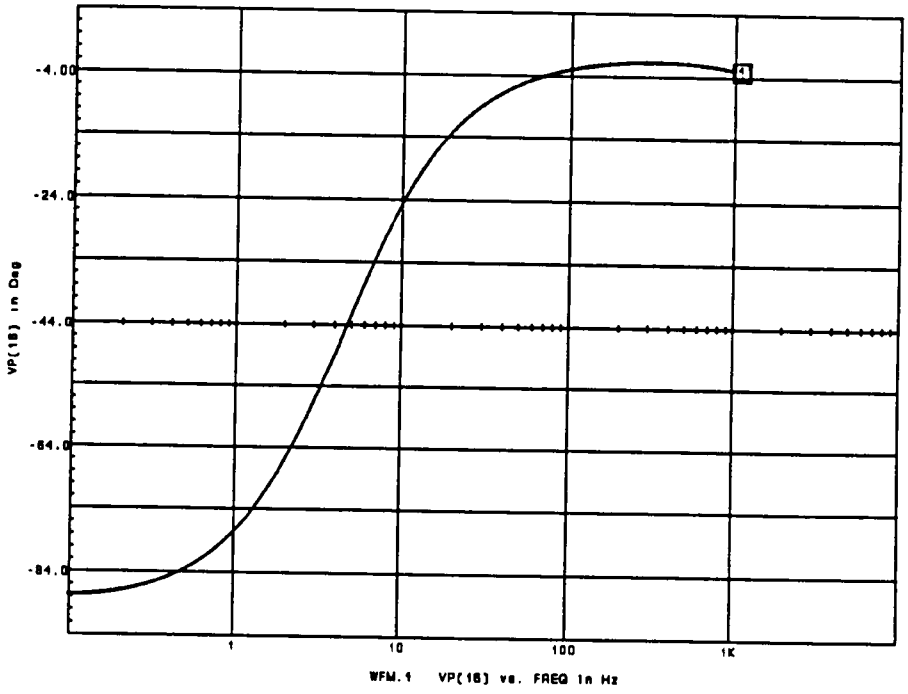


Figure 4-7, Phase plot of controller transfer function.

CHAPTER 5

SYSTEM SIMULATION: SECOND ORDER EFFECTS

5-1 Derivation of Ripple Torque Equation

The parameters used in the last chapter were assumed to be static. Particularly, the torque constant K_t was given a fixed value for use in the linear simulation. In practice, electric motors inherently have a certain amount of ripple torque. The ripple torque for a DC motor has the shape of a full wave rectifier process. In particular, the torque ripple for the motor used in the ADM is shown in Fig. (5-1).

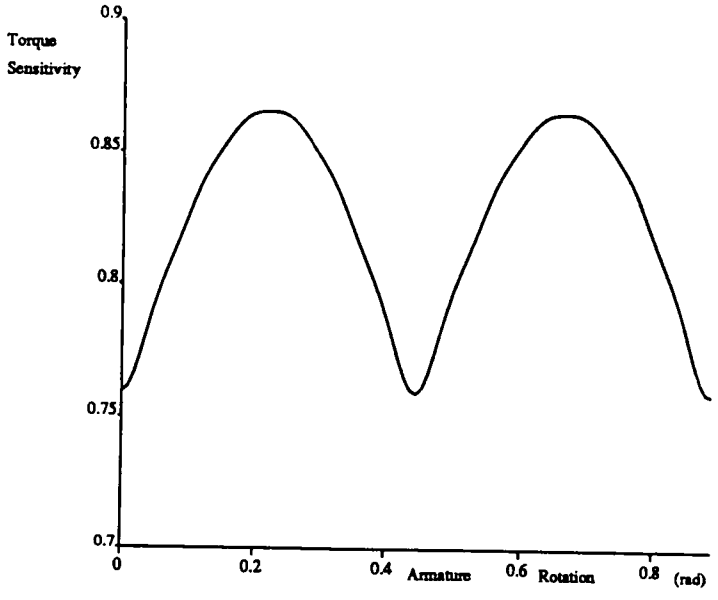


Figure 5-1, Ripple torque.

The waveform shown in Fig. (5-1) may be represented by a Fourier series, this series will be used in the simulation as a substitution for the torque constant K_t . The Fourier series representing the ripple torque is given as eq. (5-1).

$$K_t(\theta) = T_{min} + 2\frac{(T_{max} - T_{min})}{\pi} + 4\frac{(T_{max} - T_{min})}{\pi} - \sum_{n=1}^{\infty} \frac{Cos\ (n\ K_r\ \theta)}{4n^2 - 1} \quad (5\text{-}1)$$

Where,

T_{max} = *maximum torque*

T_{min} = *minimum torque*

θ = *motor position*

K_r = *frequency constant* $\left(\frac{cyc}{rad}\right)$

By substituting the values given in the Inland motor catalog [8] for the QT5404-B, and truncating the series after the sixth term, eq. (5-1) becomes:

$$K_t(\theta) = (.754) - .142\left[\frac{1}{3}Cos(14.17\ \theta) + \frac{1}{15}Cos(28.34\ \theta) + \frac{1}{35}Cos(42.51\ \theta) + \frac{1}{63}Cos(56.68\ \theta) + \frac{1}{99}Cos(70.85\ \theta) + \frac{1}{143}Cos(85.02\ \theta)\right]$$

The above equation can be substituted into to the SIMNON code to represent the effect of the varying torque constant K_t . The complete SIMNON code is given in Appendix A for both the linear and the non-linear simulation. The next section will add the effects of backlash and saturation to complete the model for the nonlinear system.

5-2 Backlash and Saturation Equations

The effects of backlash and saturation must be included in the modeling of any real world application. Neglecting these effects will result in erroneous results due to the physical constraints indicative of amplifiers and motors. Particularly, the controller designed in this thesis employs an extremely large DC gain which would imply an equally large error signal which would cause the amplifier or motor driver to saturate. Even if the amplifier possessed a large output compliance, the flux in the air gap of the motor would saturate due to the large impressed voltage. These effects are easily handled in SIMNON by using simple " if then else" statements. These statements will not be developed here but, are shown in the SIMNON code given in Appendix A.

5-3 Addition of Disturbance Torque

With the addition of the secondary effects, the response of the system changes dramatically. The introduction of the disturbance torque introduces zeros in the closed loop response, causing a high frequency oscillation in the transient portion of the system response as depicted by the solid black area in Fig. (5-2a). Figure 5-2a shows that the error settles in approximately 400 milliseconds which is within the specifications set forth in section 3-2. The lag controller actually amplifies the effect of the disturbance torque rather than reducing it, the short transient period of the error response is not a serious problem in the ADM because of the nature of the machining process. The tool slide is generally set into motion before any cutting of the material begins; therefore, the error due to the disturbance torque will not affect the surface finish of the workpiece.

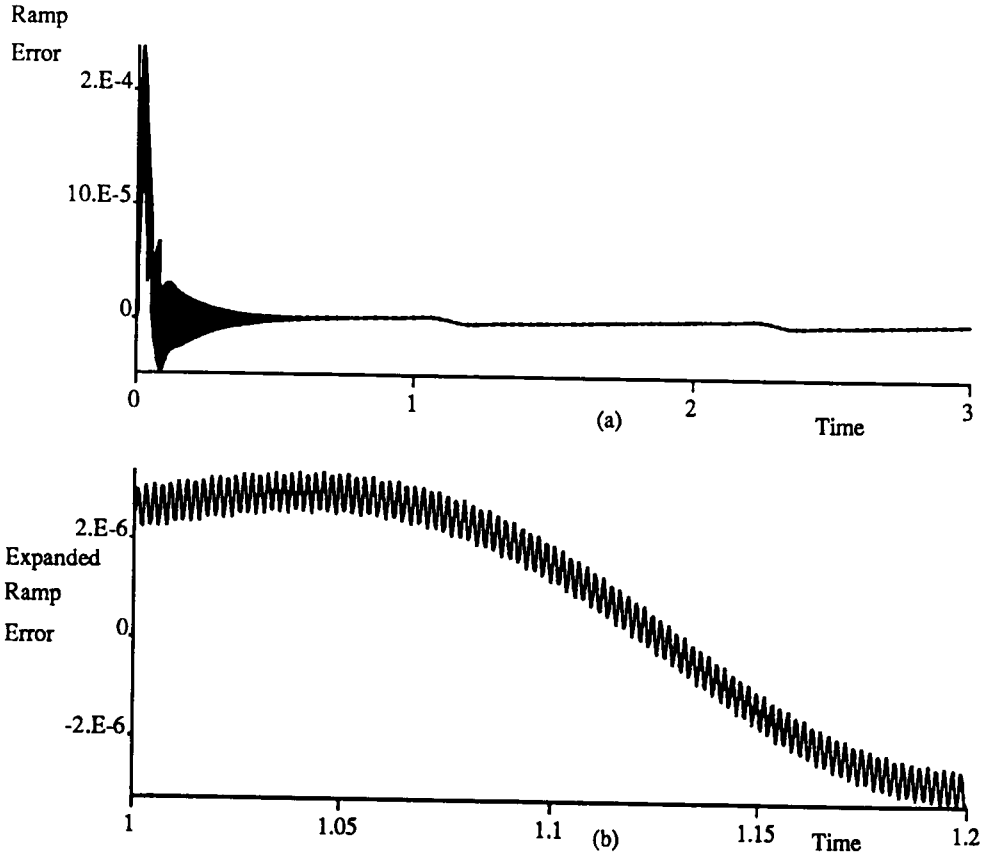


Figure 5-2, Error response due to ramp function input:
(a) error response, (b) expanded error response.

5-4 Addition of Ripple Torque

The effect of adding the ripple torque can be seen in Figs. (5-2a) and (5-2b), unfortunately the ripple torque gives rise to a cyclical error. Figure (5-2b) shows an expanded view of the error around one of the points where the torque is reaching a minimum. The error in the steady state is within the specification but, the cyclical error is approximately 5 times the desired error of 1 μ inch. This cyclical error will cause an unacceptable imperfection on the surface of the workpiece.

5-5 Addition of Backlash and Saturation

The transient error response depicted in Fig. (5-2a) reveals a discontinuity at approximately 100 milliseconds, this discontinuity is due to the saturation of the amplifiers which must be clamped to the 30 volt bus to prevent the core of the servo motor from saturating. The workpiece should be unaffected by this discontinuity, due to the fact that this discontinuity occurs during the transient portion of the response. The other consequence of saturation is revealed in the step response shown in Appendix A as Fig. A-1. The step response plot reveals that the response of the system due to a large command signal causes the output of the system to be similar to a ramp response until the amplifiers return to linear operation. This ramp response can be reduced or even eliminated if the command signal is kept to a reasonable value so as to not drive the amplifiers to the 30 volt bus. Of course, the step function as a control signal would cause severe discontinuities on the surface of the workpiece if the diamond tool bit was touching the surface; thus, the step function would only be used as a means to position

the tool holder before any cutting action occurs.

Similarly, the introduction of the one degree of backlash does not affect the system once the tool holder is in motion. If more than one degree of backlash is introduced into the system , the system may need some type of pre-load or pre-positioning to diminish the delay of the response.

5-6 Motor Constraints

The servo motor used in the control of the ADM develops a peak torque of 5.0 pound feet. This peak torque is developed with the applied voltage of 30 VDC, and a peak current of 6.15 amperes. The motor power must be kept within these constraints, except for short duty cycles, in order to prevent the servo motor from thermal destruction. Figures 5-3 a and b, show the motor current and the motor power respectively for a ramp signal with a slope of 0.01. If the slope of the ramp signal is increased, excessive motor power will be absorbed causing the destruction of the motor.

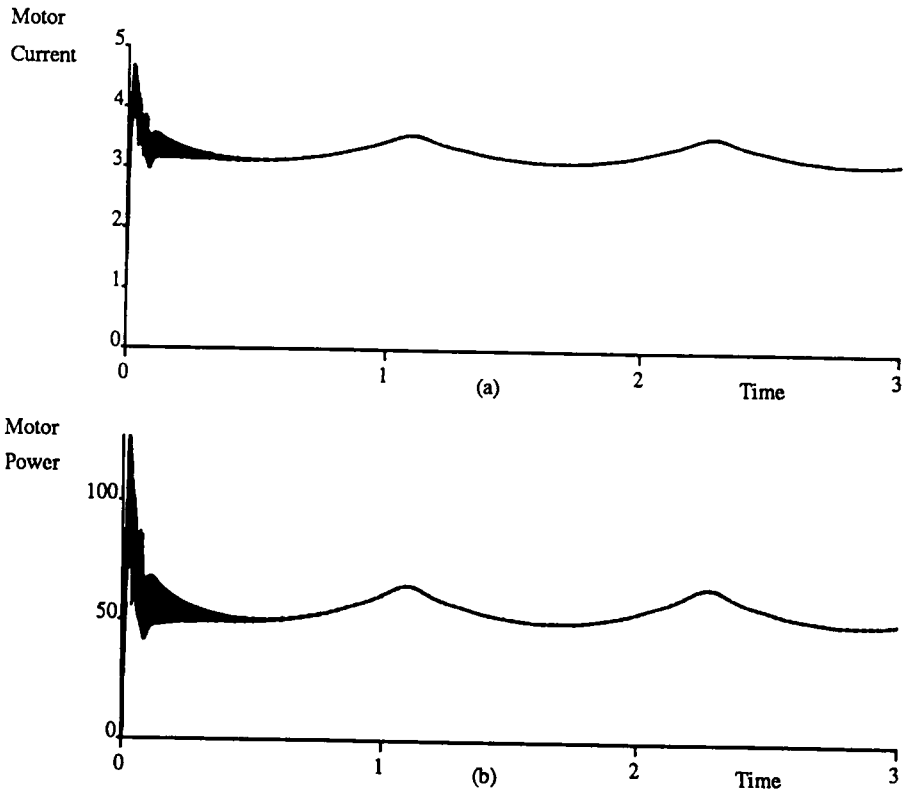


Figure 5-3, Response due to ramp function input:
(a) Motor current, (b) Motor power.

CONCLUSION

The study of the ADM was performed to establish a basis as to whether or not a machine of its size could be controlled precisely. The specifications were not firmly known to determine what parameters could be changed or to what extent the system must rely on electrical compensation.

The simulations proved to be indispensable in gaining an understanding of the way the system responded to parametric changes. The assumptions used in explaining the secondary effects are valid only if the machine tool is not in contact with the surface as the command signal begins. This assumption may be flawed if the workpiece is machined in both directions. If the leadscrew is reversed while the machine tool is in contact with the workpiece, the transient portion of the response will have a profound negative impact on the workpiece surface.

The addition of the lag controller proved to give satisfactory results in the response of the linear system. The problem in meeting the error specification arose when the ripple torque was introduced into the motor model. The ripple torque caused a cyclical error to appear in the toolholder position; therefore, causing an error to appear on the workpiece. The error introduced in the surface finish of the workpiece is not acceptable. To counteract the negative effect of the ripple torque and to improve the overall system response, the following suggestions are made:

1. Increase the gain of the lag controller to decrease the error further. This will, of course, increase the overshoot.

2. Decrease the weight of the toolholder to 30 pounds; thereby, decreasing the load inertia. This will decrease the oscillations in the transient portion of the system response.

3. Replace the servo motor with a unit that possesses a smoother torque profile. The above suggestions may or may not be economically feasible due to the nature of changing the hardware.

Further study should be aimed at improving the system response in the presence of the disturbance torque as well as any sensor noise. The foregoing suggestions should be implemented on the mock-up machine to ascertain the accuracy of the modeling. Should the model prove to be accurate, the design of an additional or new controller is easily accomplished since most of the simulation code is already written. The design of a new controller should take in account, the disturbance torque as well as the command input. The design should be performed for a MISO system using a technique such as quantitative feedback theory (QFT) [7], this unified technique allows both inputs to be taken into account simultaneously; thus, providing not only a good position controller but one that rejects the disturbance torque. Once the transfer function for the controller is determined, it should be transformed into a digital controller so that it may be implemented on a microcontroller.

LIST OF REFERENCES

LIST OF REFERENCES

[1] Bailey, J. Milton. Advanced Diamond Machining Systems. Research Proposal., University of Tennessee., 1988

[2] Douglass, S. Stevens. A Machining System For Turning Nonaxisymetric Surfaces. PhD. Dissertation., University of Tennessee., 1983

[3] Elmqvist, Hilding and K. Johan Astrom. Simnon User's Guide. Lund Institute of Technology., Lund, Sweden., 1986

[4] Kuo, Benjamin C. Automatic Control Systems. Prentice Hall, Inc., Englewood, NJ., 1982

[5] PC-Matlab User's Guide. The Math Works, Inc., Natick, MA., 1990

[6] Franklin, G.F., Powell J.D., and Emami-Naeini, A. Feedback Control of Dynamic Systems. Addison-Wesley Publishing Co., Reading, MA., 1986

[7] D'Azzo, John J. and Constantine H. Houpis. Linear Control System Design and Analysis. McGraw Hill Book Co., New York, NY., 1988

[8] Inland Motor Specialty Products Group. Direct Drive DC Motors. Kollmorgen Corp. Radford, VA., 1985

[9] Kuo, Benjamin C., Tal Jacob Incremental Motion Control SRL Publishing Co., Champain, Ill., 1978

[10] Universal Thread Grinding Company. Precision Leadscrews . Fairfield, Ct., 1988

APPENDICES

APPENDIX A

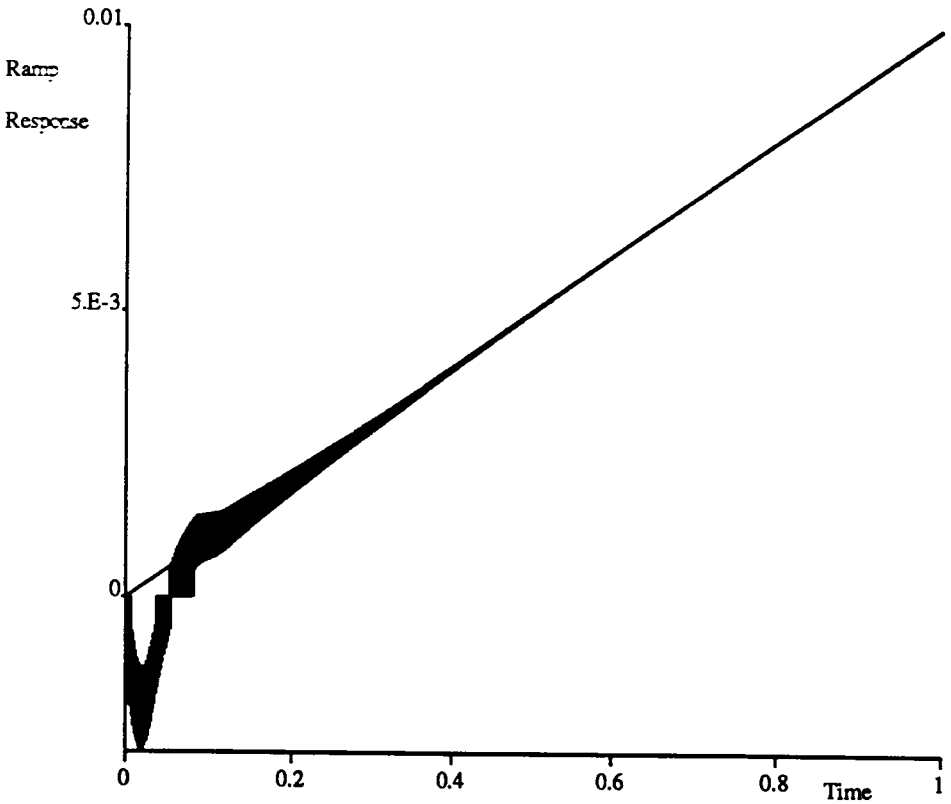


Figure A-1, Tool holder position with ramp function input.

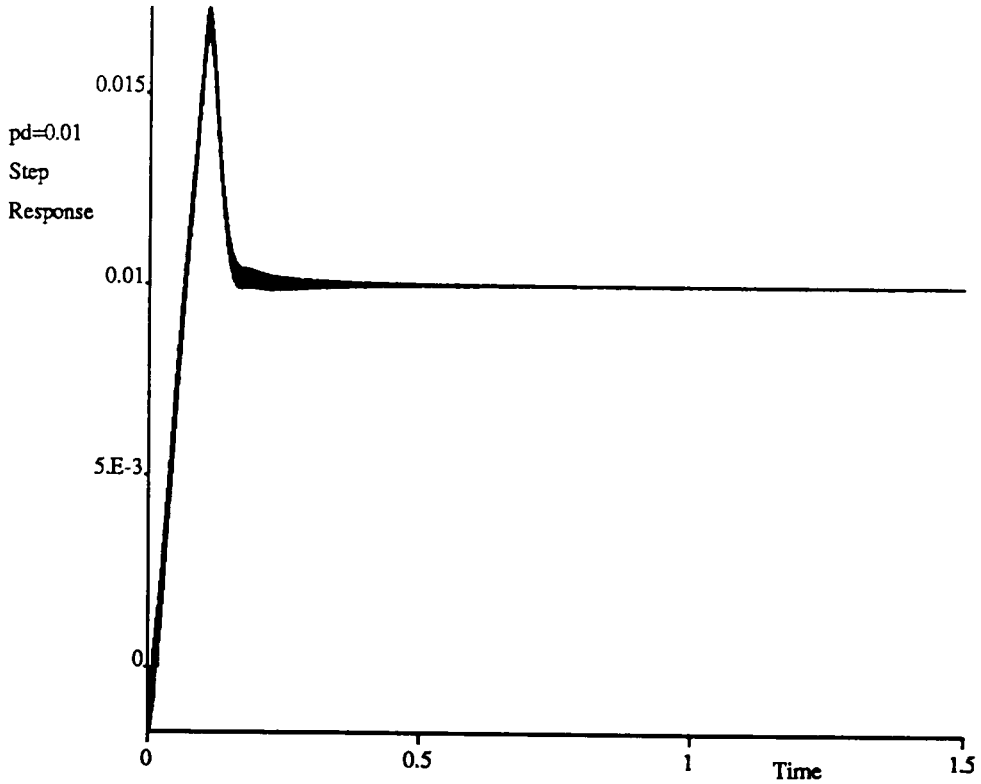


Figure A-2, Tool holder position with step function input.

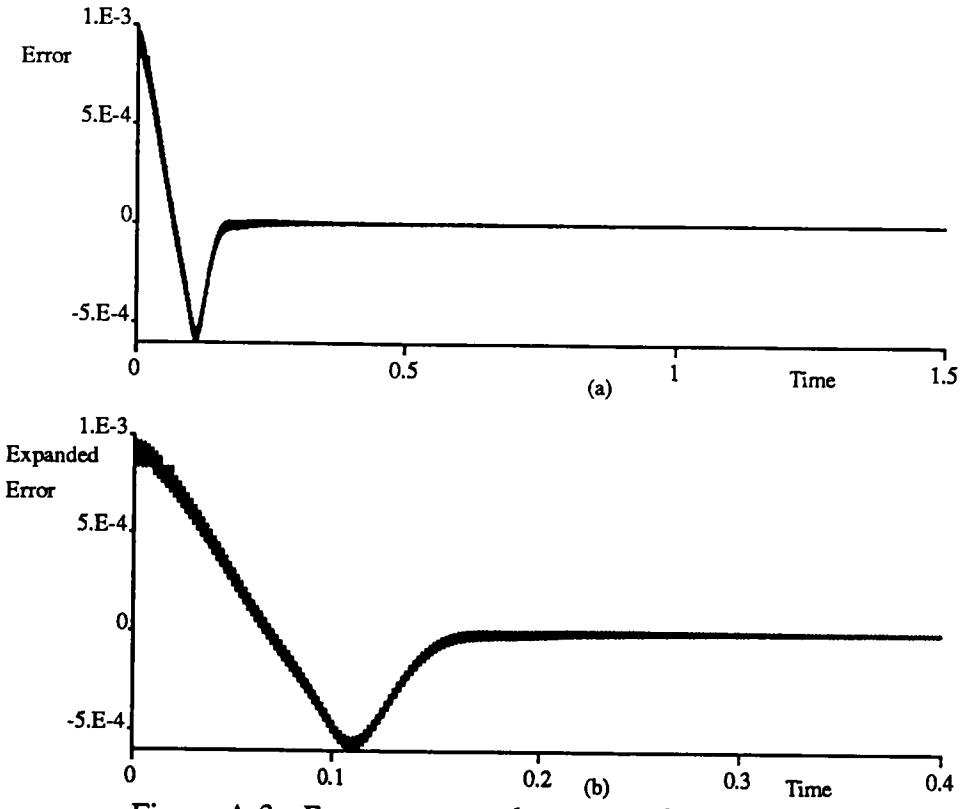


Figure A-3, Error response due to step function input:
(a) Error, (b) Expanded error.

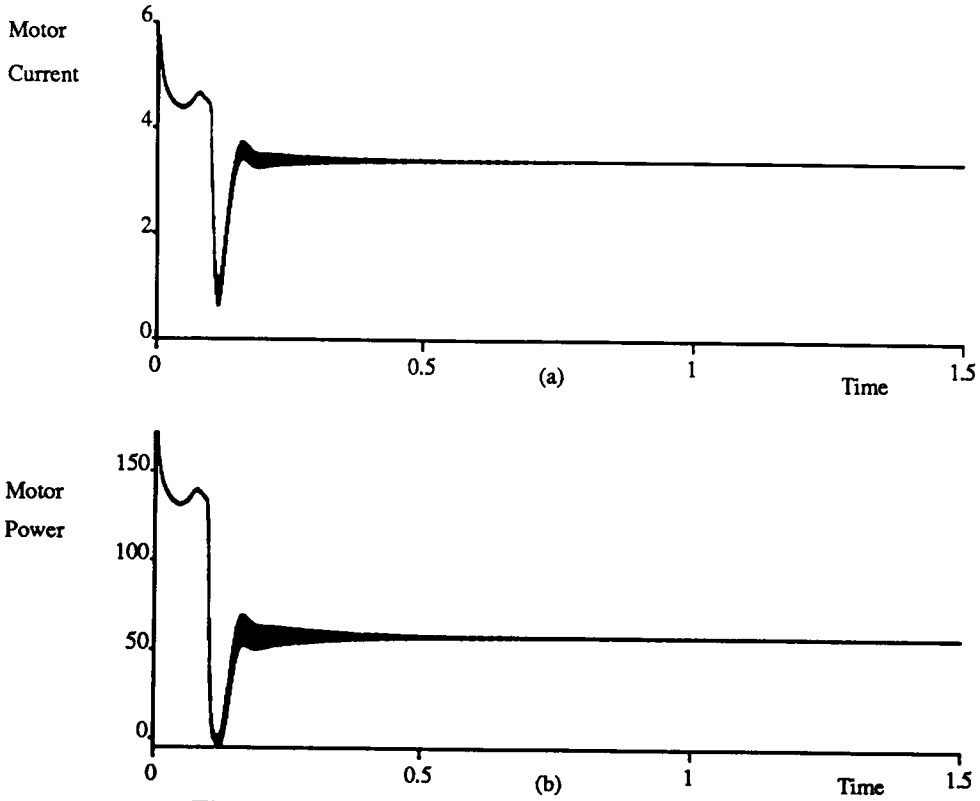


Figure A-4, Response due to step function input:
(a) Motor current, (b) Motor power.

APPENDIX B

Files necessary to run simulations:

System- Ramp response for non-linear system

Macro- admrnl.t
Driving- admrmp.t
Controller- admlag.t
Plant- admpnl.t
Connecting- admrnc.t

System- Ramp response for linear system

Macro- admrl.t
Driving- admrmp.t
Controller- admlag.t
Plant- admpl.t
Connecting- admrlc.t

System- Step response for non-linear system

Macro- admsnl.t
Driving- admstp.t
Controller- admlag.t
Plant- admpnl.t
Connecting- admsnc.t

System- Step response for linear system

Macro- admrsl.t
Driving- admstp.t
Controller- admlag.t
Plant- admpl.t
Connecting- admslc.t

Plants:

```
CONTINUOUS SYSTEM admpnl
TIME t
INPUT Va "motor voltage"
OUTPUT lp ro pos rpos thp Pm Kt lv"output variable declerations"
STATE lsp lsv Ia mpos msp "leadscrew pos. leadscrew vel."
DER dlsp dlsv dIa dmpos dmsp
"
"State equations
"
dlsp=lsv
dlsv=(1/jl)*(-tl-bl*lsv+kc*mpos-kc*lsp)
dmpos=msp
dmsp=(1/jm)*(tg-bm*msp-kc*mpos+kc*lp-tf)
dIa=((Vac-Vg)-Ia*Ra)/Lm
"limiter for output amplifier"
Vac=if Va>msat then msat else if Va<-msat then -msat else Va
"Vac=Va
"backlash of leadscrew to tool holder"
"
Pm=Ia*Vac       "motor power"
Tg=Kt*Ia        "motor torque"
Vg=kb*msp       "back emf generation"
out=if lsp>b then lsp else if lsp<-b then lsp else 0
thp=out*kp    "rotary to translational motion conversion"
kp=pitch/(2*pi)
jl=(thw*kp^2)/g   "load inertia referenced to leadscrew"
tl=((fn*dm)/2)*((tanalpha+f)/(1-f*tanalpha))  "load torque calc."
fn=(wm^2*ro*thw)/g
tanalpha=(pitch/(pi*dm))
ro=(6.561-thp)    "position of leadscrew from maximum pos."
pos=ro*304.8      "conversion from ft. to mm."
rpos=thp*12
"Torque ripple equation
Kt=Tmin+((2*(Tmax-Tmin))/pi)-((4*(Tmax-Tmin))/pi)*p1
p1=(1/3)*Cos(Kr*mpos)+(1/15)*Cos(2*Kr*mpos)+p2
p2=(1/35)*Cos(3*Kr*mpos)+(1/63)*Cos(4*Kr*mpos)+p3
p3=(1/99)*Cos(5*Kr*mpos)+(1/143)*Cos(6*Kr*mpos)
"
lp=lsp
lv=lsv "lead screw velocity"
"constants
"
```

```
Kr:14.17
Tmax:.866
Tmin:.754
msat:30      "saturation of output amp
b:17.45e-3    "backlash 1 degree
thw:50      "tool holder weight (lbs.)"
g:32.15     "gravitational force (ft/s^2)"
pitch:.0139   "lead screw pitch in (ft.)"
pi:3.14159
dm:40.66e-3   "mean shaft dia. in (ft)
bl:.0001      "viscous damping of the load"
f:.001      "coeff. of static friction of leadscrew"
wm:10.47      "main spindle speed (rad/s)"
Lm:3.6E-3 "armature inductance (henries)"
kb:1.1        "back emf constant"
bm:.153       "damping coeff."
jm:1.9e-3     "motor inertia"
tf:.15        "static friction
kc:78.665     "shaft spring constant"
Ra:5    "armature resistance (ohms)"
END

CONTINUOUS SYSTEM admpl
TIME t
INPUT Va "motor voltage"
OUTPUT lp ro pos rpos thp Pm "output variable declerations"
STATE lsp lsv Ia mpos msp "leadscrew pos. leadscrew vel."
DER dlsp dlsv dIa dmpos dmsp

"State equations

dlsp=lsv
dlsv=(1/jl)*(-tl-bl*lsv+kc*mpos-kc*lsp)
dmpos=msp
dmsp=(1/jm)*(tg-bm*msp-kc*mpos+kc*lp-tf)
dIa=((Vac-Vg)-Ia*Ra)/Lm
Vac=Va
Pm=Ia*Vac      "motor power"
Tg=Kt*Ia       "motor torque"
Vg=kb*msp      "back emf generation"
thp=lsp*kp    "rotary to translational motion conversion"
kp=pitch/(2*pi)
jl=(thw*kp^2)/g   "load inertia referenced to leadscrew"
tl=0
```

```
ro=(6.561-thp)    "position of leadscrew from maximum pos."
pos=ro*304.8      "conversion from ft. to mm."
rpos=thp*12
lp=lsp
"constants
thw:50      "tool holder weight (lbs.)"
g:32.15     "gravitational force (ft/s^2)"
pitch:.0139   "lead screw pitch in (ft.)"
pi:3.14159
dm:40.66e-3   "mean shaft dia. in (ft)
bl:.0001      "viscous damping of the load"
f:.001      "coeff. of static friction of leadscrew"
wm:10.47      "main spindle speed (rad/s)"
Lm:3.6E-3 "armature inductance (henries)"
Kt:.810   "torque sensitivity"
kb:1.1          "back emf constant"
bm:.153         "damping coeff."
jm:1.9e-3       "motor inertia"
tf:.15          "static friction
kc:78.665       "shaft spring constant"
Ra:5     "armature resistance (ohms)"
END
```

Driving Functions:

```
CONTINUOUS SYSTEM admrmp
TIME t
output vd
vd=if t>0 then t/s else 0
s:100
end
```

```
CONTINUOUS SYSTEM admstp
TIME t
output vd
vd=if t>0 then 1/s else 0
s:100 "position constant
End
```

Macros:

```
MACRO admrnl
syst admrmp admlag admpnl admrnc
store rpos ia e pd pm lv
```

```
END

MACRO admrl
syst admrmp admlag admpl admrlc
store rpos ia e pd
END

MACRO admsnl
syst admstp admlag admpnl admsnc
store rpos ia e pd pm
END

MACRO admsl
syst admstp admlag admpl admslc
store rpos ia e pd vac
END
```

Connecting systems:

```
CONNECTING SYSTEM admrnc
TIME t
pd[admlag]=vd[admrmp]
feed[admlag]=rpos[admpnl]
va[admpnl]=vo[admlag]
END

CONNECTING SYSTEM admsnc
TIME t
pd[admlag]=vd[admstp]
feed[admlag]=rpos[admpnl]
va[admpnl]=vo[admlag]
END

CONNECTING SYSTEM admrlc
TIME t
pd[admlag]=vd[admrmp]
feed[admlag]=rpos[admpl]
va[admpl]=vo[admlag]
END

CONNECTING SYSTEM admslc
TIME t
pd[admlag]=vd[admstp]
feed[admlag]=rpos[admpl]
```

```
va[admpl]=vo[admlag]
END
```

Control:

```
CONTINUOUS SYSTEM admlag
TIME t
OUTPUT vo e
INPUT feed pd
STATE x1
DER dx1
dx1=k*vi-p*x1
vi=(pd-feed)/12
e=vi
vo=(z-p)*x1+k*vi
"CONSTANTS
k:85e3
z:30
p:.01
END
```

Matlab Files:

```
% Matlab Mfile for Advanced Diamond Machining
% System with  controller gain, unity feedback, theta in rad
% Define constants
format short e
Lm=.0036; Ra=5;
Kt=.810; Jm=.0019;
Bm=.153; Kc=78.665;
Jl=36.79E-6; Bl=.0001;
Kb=1.1; Gc=100e3;
%Variables
G=Jl*Jm*Lm
C5=1
C4=(Bl*Jm*Lm+Bm*Jl*Lm+Jl*Jm*Ra)/G
C3=(Bl*(Bm*Lm+Jm*Ra)+Bm*Jl*Ra+Jl*(Kb*Kt+Kc*Lm)+Jm*Kc*Lm)/G
C2=(Bl*(Bm*Ra+Kb*Kt+Kc*Lm)+Bm*Kc*Lm+Jl*Kc*Ra+Jm*Kc*Ra)/G
C1=(Bl*Kc*Ra+Bm*Kc*Ra+Kb*Kc*Kt)/G
C0=(Kt*Kc*Gc*2.212e-3)/G
num=C0;
den=[C5 C4 C3 C2 C1 C0];
roots(den)
t=0:.001:.1;
```

```
u=t;
plot(t,step(num,den,t));
xlabel('Time');ylabel('Position');title('Step response');
meta admcls.met
pause
[Y,X]=lsim(num,den,u,t);
plot(t,Y,t,t)
xlabel('Time');ylabel('Position');title('Ramp response');
meta admclr.met

% Matlab Mfile for Advanced Diamond Machining
% Define constants
Lm=.0036; Ra=5;
Kt=.810; Jm=.0019;
Bm=.153; Kc=78;
Jl=36.79E-6; Bl=.0001;
Kb=1.1; Gc=50e3;
n=100;
%Variables
Ck=Jl*Jm*Lm;
C5=1;
C4=(Bl*Jm*Lm+Bm*Jl*Lm+Jl*Jm*Ra)/Ck;
C3=(Bl*(Bm*Lm+Jm*Ra)+Bm*Jl*Ra+Jl*(Kb*Kt+Kc*Lm)+Jm*Kc*Lm)/Ck;
C2=(Bl*(Bm*Ra+Kb*Kt+Kc*Lm)+Bm*Kc*Lm+Jl*Kc*Ra+Jm*Kc*Ra)/Ck;
C1=(Bl*Kc*Ra+Bm*Kc*Ra+Kb*Kc*Kt)/Ck;
C0=(Kt*Kc*Gc*.002212)/Ck;
num=C0;
den=[C5 C4 C3 C2 C1 0];
roots(den)
k=0:n;
r=rlocus(num,den,k);
% Placing r matrix in column vector form
for i=1:n+1,
        r1(i)=r(i,1);
        r2(i)=r(i,2);
        r3(i)=r(i,3);
        r4(i)=r(i,4);
        r5(i)=r(i,5);
end
% Checking approximate jw-axis crossing
k1=Gc*(min(find((real(r1))>0))-1)
k2=Gc*(min(find((real(r2))>0))-1)
k3=Gc*(min(find((real(r3))>0))-1)
k4=Gc*(min(find((real(r4))>0))-1)
```

```
k5=Gc*(min(find((real(r5))>0))-1)
plot(r,'.')
xlabel('Real axis'),ylabel('Imag. axis')
title('Root locus plot')
meta rl.met
%t=0:.0001:.1;
%plot(t,step(num,den,t));
v=[-1500,500,-2000,2000];
axis(v)
pzmap(num,den)
title('Pole-zero plot')
meta pz.met
clear
pause

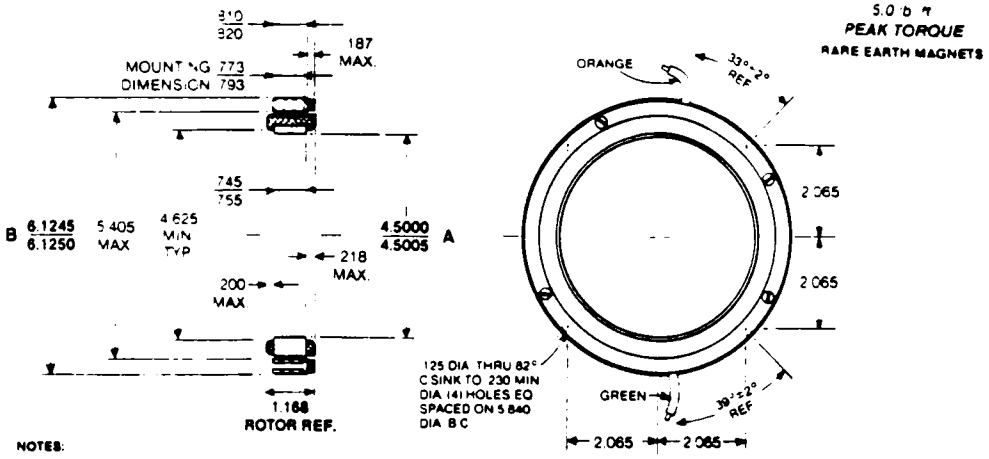
% Matlab Mfile for Advanced Diamond Machining
% Define constants
C0=2.048e12;
C6=1;
C5=1472.01;
C4=24.26e5;
C3=32e8;
C2=51.78e10;
C1=51.78e8;
n=200;
num=C0*[1 30];
den=[C6 C5 C4 C3 C2 C1 0];
roots(den)
k=0:n;
v=[-1500,500,-2000,2000];
axis(v)
r=rlocus(num,den,k);
plot(r,'.')
grid
xlabel('Real axis'),ylabel('Imag. axis')
title('Root locus plot')
pause
meta rl.met
pzmap(num,den)
title('Pole-zero plot')
meta pz.met
clear
pause
```

Spice file:

```
thesis
*SPICE_NET
*INCLUDE LIN.LIB
 DEC 100 .01 1K
TIONS LIMPTS=5000
*ALIAS  V(5)=VO
*ALIAS  V(4)=VI
*ALIAS  V(16)=VO2
R1 1 0 51
R2 3 4 51
R3 3 6 1.5MEG
R4 6 5 510
C1 3 6 68UF
V1 4 0 AC 1
R5 5 8 1.2K
V2 13 0 DC 15
V3 0 7 DC 12
X2 8 11 14 13 10 LF156
R6 8 14 110K
R7 11 0 1K
V4 0 10 DC 12
V5 12 0 DC 15
X3 15 14 16 2 9 LF156
R9 15 0 1.2K
R10 15 16 110K
V6 2 0 DC 15
V7 0 9 DC 15
R11 16 0 100K
X1 3 1 5 12 7 LF156
END
```

QT-5404

5.0 oz-ft
PEAK TORQUE
RARE EARTH MAGNETS



NOTES:

1 – MOTOR TO BE SHIPPED AS THREE SEPARATE COMPONENTS BRUSH RING ASSEMBLY ROTOR ASSEMBLY AND STATOR ASSEMBLY
2 – MOUNTING REQUIREMENTS DIAMETERS 'A' AND 'B' TO BE CONCENTRIC WITHIN .002 (.004 T.I.R.) WHEN MOUNTED
3 – WITH POSITIVE CURRENT APPLIED TO GREEN LEAD WITH RESPECT TO ORANGE LEAD ROTATION SHALL BE C.W. FACING BRUSH RING END
4 – TYPICAL BRUSH LIFE – 10⁸ REVS

LEADS
#20 AWG 19-STRAND TYPE E TEFLON COATED PER MIL W-16878/12 MIN LG

SIZE CONSTANTS

		Value	Units
Peak Torque Rating - T_P		5.0	LB. FT.
Power Input, Stalled at T_H(25°C) - P_P		227	WATTS
Motor Constant - K_M		0.33	LB.FT./$\sqrt{\text{WATT}}$
No Load Speed, Theoretical @ V_P - ω_{NL}		33	RAD/S
Electrical Time Constant - t_E		0.60	MS
Static Friction (Max.) - T_F		0.15	LB. FT.
Viscous Damping Coefficients	Zero Impedance - F_0	0.15	LB. FT. PER RAD/S
	Infinite Impedance - F_I	0.003	LB. FT. PER RAD/S
Maximum Winding Temperature		155	°C
Temperature Rise per Watt - TPR		2.0	°C/WATT
Ripple Torque (Average to Peak) - T_R		7	PERCENT
Ripple Frequency (Fundamental)		89	CYCLES/REV.
Number of Poles		20	
Rotor Inertia - J_M		1.9×10^{-3}	LB.FT.S²
Motor Weight		2.9	LB.

WINDING CONSTANTS — Winding Designation

	UNITS	TOLERANCES	A	B	C	D	E	F	G
Voltage, Stalled at T_H(25°C) - V_P	VOLTS	Nom.	18.5	30.8	24.6	64.9	51.6	40.6	
Peak Current - I_P	AMPERES	Rated	12.3	6.15	7.94	3.09	3.97	5.00	
Torque Sensitivity - K_T	LB.FT./AMP	±10%	0.405	0.810	0.630	1.62	1.26	1.00	
Back EMF Constant - K_B	V per RAD/S	±10%	0.549	1.10	0.854	2.20	1.71	1.36	
DC Resistance (25°C) - R_M	OHMS	±12.5%	1.50	5.00	3.10	21.0	13.0	8.11	
Inductance - L_M	mH	±30%	0.90	3.6	2.2	14	8.8	5.5	

VITA

Daniel Steven Daniel, was born in Baltimore, Maryland on December 14, 1959. He attended both private and public elementary schools in Woodlawn, Maryland. He then attended both Pikesville Jr. and Sr. High schools in Pikesville, Maryland where he graduated in June of 1978. After graduating, he began to work as a technician in the electric motor service industry.

After four years of working in the service industry, Mr. Daniel began attending the Catholic University of America in Washington, D.C. majoring in Electrical Engineering. After graduating in the spring of 1986, he accepted a position with the Murray Corporation in Hunt Valley, Maryland where he was employed for one year as a development engineer. He then was employed by the Black and Decker Manufacturing Co. in Towson, Maryland where he was employed for two years before entering the University of Tennessee-Knoxville in the Fall of 1988.

Mr. Daniel was then employed part time by Martin Marietta Energy Systems in Oak Ridge, Tennessee. In August of 1990, Mr. Daniel left Tennessee to pursue work in various industries around the United States. In the summer of 1993, he returned to the University of Tennessee to complete his education. In the fall of 1993, Mr. Daniel received his Master of Science degree in Electrical Engineering.

Currently, Mr. Daniel is enrolled in the Doctoral Program in Electrical Engineering at UTK, and also holds the position of Development Associate II at the Oak Ridge National Laboratory in Oak Ridge, Tennessee.